Heliyon 9 (2023) e18363

Contents lists available at ScienceDirect

Heliyon

journal homepage: www.cell.com/heliyon

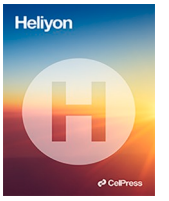

# Box-Behnken modeling to quantify the impact of control parameters on the energy and tensile efficiency of PEEK in MEX 3D-printing

Nectarios Vidakis [a], Markos Petousis [a,*], Nikolaos Mountakis [a], Emmanuel Karapidakis [b]

[a] Department of Mechanical Engineering, Hellenic Mediterranean University, Heraklion, 71410, Greece
[b] Electrical and Computer Engineering Dept., Hellenic Mediterranean University, Heraklion, 71410, Greece

ARTICLE INFO

*Keywords:*
Polyetheretherketone (PEEK)
Box-Behnken
Energy consumption
Mechanical response
Material extrusion
Fused filament fabrication (FFF)
3D printing

ABSTRACT

Currently, energy efficiency and saving in production engineering, including Material Extrusion (MEX) Additive Manufacturing, are of key importance to ensure process sustainability and cost-effectiveness. The functionality of parts made with MEX 3D-printing remains solid, especially for expensive high-performance polymers, for biomedical, automotive, and aerospace industries. Herein, the energy and tensile strength metrics are investigated over three key process control parameters (Nozzle Temperature, Layer Thickness, and Printing Speed), with the aid of laboratory-scale PEEK filaments fabricated with melt extrusion. A double optimization is attempted for the production by consuming minimum energy, of PEEK parts with improved strength. A three-level Box-Behnken design with five replicas for each experimental run was employed. Statistical analysis of the experimental findings proved that LT is the most decisive control setting for mechanical strength. An LT of 0.1 mm maximized the tensile endurance (~74 MPa), but at the same time, it was responsible for the worst energy (~0.58 MJ) and printing time (~900 s) expenditure. The experimental and statistical findings are further discussed and interpreted using fractographic SEM and optical microscopy, revealing the 3D printing quality and the fracture mechanisms in the samples. Thermogravimetric analysis (TGA) was performed. The findings hold measurable engineering and industrial merit, since they may be utilized to achieve an optimum case-dependent compromise between the usually contradictory goals of productivity, energy performance, and mechanical functionality.

## 1. Introduction

In recent years, AM has become one of the most rapidly expanding technologies with growing engineering notice and industrial exploitation [1]. It is also considered an eco-friendly process, owing to its reduced energy consumption and minimized waste, compared to other more traditional manufacturing technologies [2]. Nevertheless, the sustainability of AM remains an open issue that is usually investigated in the literature [1,3]. One of the most dominant factors, especially nowadays, that affects the sustainability and

* Corresponding author.
*E-mail addresses:* vidakis@hmu.gr (N. Vidakis), markospetousis@hmu.gr (M. Petousis), mountakis@hmu.gr (N. Mountakis), karapidakis@hmu.gr (E. Karapidakis).

https://doi.org/10.1016/j.heliyon.2023.e18363
Received 15 January 2023; Received in revised form 28 April 2023; Accepted 14 July 2023
Available online 17 July 2023

**Nomenclature**

| | |
|---|---|
| 3DP | 3D Printing |
| ABS | Acrylonitrile Butadiene Styrene |
| AM | Additive Manufacturing |
| ANOVA | Analysis of Variances |
| BB-DOE | The Box-Behnken design of the experiment |
| BT | Bed Temperature |
| DF | Degrees of Freedom |
| DOE | Design of Experiment |
| DSC | Differential Scanning Calorimetry |
| E | Tensile Modulus of Elasticity |
| EPC | Energy Printing Consumption |
| FFF | Fused Filament Fabrication |
| ID | Infill Density |
| LT | Layer Thickness |
| MEP | Main Effect Plot |
| MEX | Material Extrusion |
| NT | Nozzle Temperature |
| ORA | Orientation Angle |
| PA | Polyamide |
| PLA | Polylactic Acid |
| PEEK | Polyetheretherketone |
| PT | Printing Time |
| PS | Printing Speed |
| RDA | Raster Deposition Angle |
| QRM | Quadratic Regression Model |
| RQRM | Reduced Quadratic Regression Model |
| sB | Tensile strength |
| SEM | Scanning Electron Microscopy |
| SPE | Specific Printing Energy |
| SPP | Specific Printing Power |
| Tg | Glass Transition Temperature |
| TGA | Thermogravimetric Analysis |

the eco-friendliness of the AM processes is their energy consumption and efficiency in general [4,5]. Both are key metrics for classifying environmental footprints [6]. Several experimental approaches and modeling tools [7] have been employed, such as machine learning [8] and other statistical modeling methods, to quantify the main effects of 3D printing settings on the process energy demands [9].

MEX 3D printing is one of the most popular AM processes [10] owing to its distinctive features, which include flexibility, cost-effectiveness, and the capability to fabricate products with complicated geometrical structures [11]. This method mainly uses polymeric materials or composites, which are the most popular in the AM process [12]. Polymers such as PLA and ABS are the most widely used polymers for the MEX process [13]. They are used as pure [14–16] or matrix materials in composites [17–20]. Therefore, it is reasonable that the effects of the 3D-printer process settings on the overall performance of such feedstocks have been comprehensively investigated in previous studies [21,22]. Various modeling tools have been employed to assess and optimize the process from various perspectives [23–25].

In addition to the commonly used MEX 3D-printing filaments, high-performance polymers such as polyetheretherketone (PEEK) have been processed and investigated [26]. PEEK is a high-temperature [27], high-performance [28], biocompatible [29,30] polymer. These superior properties led to the deployment of PEEK in several types of medical applications, such as implants (surgical, cranial, lumbar, etc.) [31–33] and scaffolds [34,35] for bone regeneration [36,37]. PEEK has also been deployed in dentistry [38], where it has been proven to be equally functional as titanium-based alloys [39]. These impressive properties render PEEK polymers suitable not only for medical applications but also for the aerospace industry [40,41]. The significance of various 3D printing parameters on several responses (mechanical and thermal, etc.) of MEX 3D-made samples with PEEK has been reported in the literature [42,43]. Investigations have engaged methods such as multifactor coupling [26] and numerical modeling [28] to analyze the results and compile predictive models. Additionally, parameters affecting the efficiency of 3D printed products, such as the bonding strength in the 3D printed structure, have been reported [44]. The 3D printing settings for successfully manufacturing parts made of this polymer, that is, without warping, have also been examined [45,46]. Thermal and microstructural investigations have also been conducted to describe the thermal response of PEEK by identifying properties such as the glass transition point and other crystallinity alterations of the polymer [47]. PEEK has also been explored as a matrix material for composite development [31] with carbon-based [48,49] or other types of fillers, such as hydroxyapatite [50], to further enhance the mechanical performance of the PEEK Polymer or to induce specific

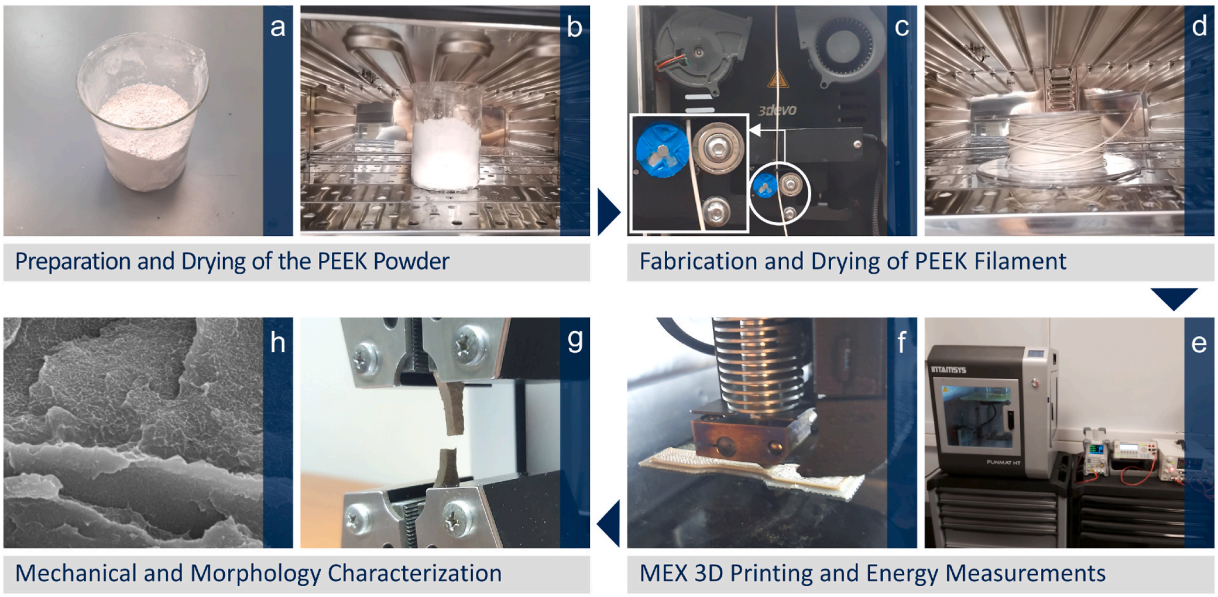


**Fig. 1.** Screenshots from the experimental course of the current research (a) raw powder material, (b) raw material drying, (c) PEEK filament extrusion, (d) feedstock drying, (e) monitoring of energy (f) samples MEX AM, (g) tensile testing, (h) morphological evaluations.

**Table 1**
VICTREX® PEEK 150UF10 properties from the material's datasheet (https://www.victrex.com/-/media/downloads/datasheets/victrex_tds_150uf10.pdf).

| Property | standard | value |
|---|---|---|
| Tensile Strength [MPa] | ISO-527 | 100.0 |
| Tensile Elongation [%] | ISO-527 | 15.0 |
| Tensile El. Modulus [GPa] | ISO-527 | 4.1 |
| Flexural Strength [MPa] | ISO-178 | 170.0 |
| Melting Point [$^{o}$C] | ISO 11357 | 343.0 |
| Glass Transition Temp. [$^{o}$C] | ISO 11357 | 143.0 |
| Density [g/cm$^{3}$] | ISO 1183 | 1.3 |

properties for particular medical applications. To depict the parameters that affect the mechanical performance of PEEK in 3D printing through MEX, modeling approaches, such as the Taguchi robust design [51,52], as well as the Box-Behnken experimental design [53,54], have been employed. Regarding the energy consumption in MEX 3D printing with PEEK filaments, the literature is still marginal, and it focuses on the energy consumption when 3D printing PEEK/carbon fiber composites by employing a full-factorial design approach [55,56].

Along with the evaluation of the mechanical response, the present research aims to provide information for process control settings that support the eco-friendliness of MEX 3D printing with PEEK. More specifically, the primary goal of this study is to optimize the control settings that minimize the energy consumption of the process. This information is not yet included in the existing literature, but it is a critical aspect of the MEX 3D printing process, considering the high temperature required for 3D printing with PEEK filaments. It is reasonable to expect substantially higher energy consumption.

Based on the literature survey presented above, the dominant 3D parameters governing the efficiency of AM workpieces made of PEEK are printing speed, layer thickness, and nozzle temperature [46,53]. The Box-Behnken experimental design was employed to analyze the experimental results [57]. In addition, to energy consumption, the effects of the selected control factors (and levels) on the mechanical strength of PEEK tensile samples made with MEX 3D printing were also quantified. This analysis was accomplished identically to the corresponding one for the energy consumption metrics, aiming to evaluate the process setting that ensures the best possible compromise between the mechanical response and energy consumption. To this end, an attempt was made to lock a set of parameters that concurrently provide the best possible mechanical performance over energy absorption. It was found that such optimization was difficult; however, the prediction models provided useful insight into the expected outcome of each metric. Therefore, the process can be optimized according to the requirements of each application, and the remaining metrics can be predicted. In this manner, users can know the expected outcomes of the process. The objectives of the study are summarized as follows.

- To evaluate the sustainability of the high-performance biomedical PEEK polymer.

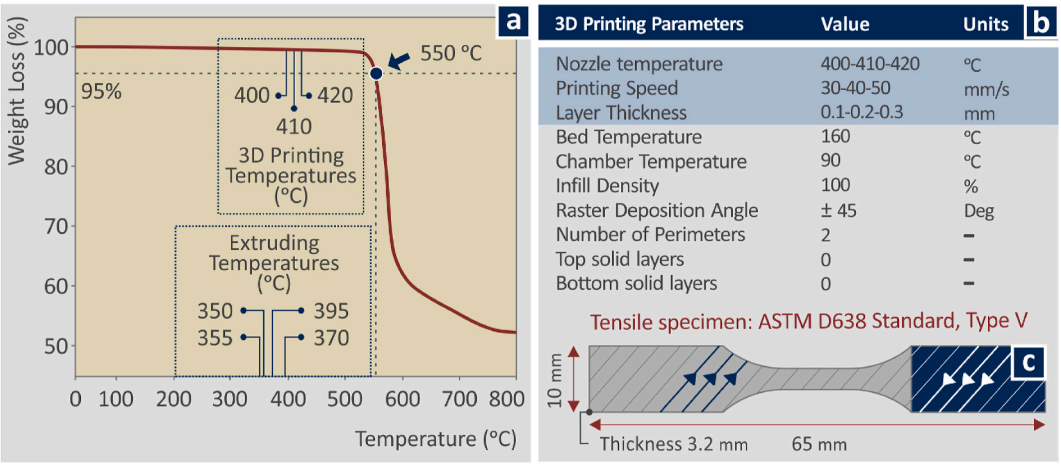


**Fig. 2.** (a) Weight loss (%) vs temperature graph (TGA) and (b) 3D printing settings for PEEK MEX and (c) specimens' geometry according to the tensile test standard (ASTM D638-02a).

- A perform a double optimization aiming to produce 3D printed parts with the PEEK polymer with increased mechanical strength and by consuming the minimum possible energy for their production. This type of double optimization has not been investigated in the PEEK polymer so far in the literature.

## 2. Materials and methods

The PEEK polymer was procured in fine-grade powder form (Fig. 1a) to be extruded in filament form suitable for 3D printing (1.75 mm diameter). The grade used was VICTREX® PEEK 150UF10 (Lancashire, United Kingdom). The technical specifications of this high-performance polymer according to the manufacturer's datasheet are listed in Table 1. This specific grade was selected for the following reasons.

- It comes from a well-respected manufacturer.
- It is suitable for extrusion (specific grades are suitable only for injection molding).
- It comes in powder form, which was the desired form for filament extrusion.
- This grade was available in the desired quantities within the schedule of the study, which is critical nowadays that there is a shortage of many products and materials.

Before the extrusion process, the PEEK powder was dried for 3 h at 150 °C according to the manufacturer's instructions (Fig. 1b). It was then extruded to the filament in a high-temperature single-screw extruder for filament production, which is thermally capable of melting PEEK polymer (3D Evo Precision 450, 3devo B.V., Netherlands, Fig. 1c). The formed filament was further dried (Fig. 1d) and fed into a high-temperature 3D printer also capable to AM process of PEEK polymer (Intamsys Funmat HT, Intamsys Technology, Shangai, China). The 3D printing settings in the study were selected based on preliminary experiments, the existing literature in the field [27,44,58], and the polymer datasheet, which suggests a processing temperature of 400 °C. The layer thickness used was the most commonly used in the literature and ensures good quality characteristics. Higher layer thickness produces more rough parts.

Throughout the 3D printing process, the printing time and consumed energy were recorded with a stopwatch (stopwatch measurement method, [59]) and Rigol DM3058E digital multimeter, respectively (RIGOL Technologies, Beijing, China, Fig. 1e). The selected control parameters are shown in Fig. 2b. Using the 3D printing process, V-type specimens with 3.2 mm thickness, after the ASTM-D638-02a norm (Fig. 2c). Five specimens were manufactured for each set of control parameters (15 runs in total were conducted in this study, with five replicates each).

The produced tensile specimens were tested according to the same standard (ASTM D638-02a) with the aid of an Imada-MX2 tester (Imada Inc., Illinois, United States), at a 10 mm/min speed of testing (strain rate) (Fig. 1g). An increasing uniaxial force load was applied in the samples until they failed in the tensile test. So, loading was not the same in all samples, it depended on the sample and its performance in the test before failure. The morphological features of the samples (fracture mechanism, etc.) were evaluated through stereoscope microscopy (OZR5 stereoscope with ODC 832 5 MP digital camera, KERN & SOHN GmbH, Germany), as well as with SEM (JSM 6362LV, Jeol, Japan). The samples were gold-coated (Au) to acquire SEM images. Images were captured in a high-vacuum state with an acceleration voltage of 20 kV (Fig. 1h). Furthermore, to ensure that the extrusion thermal settings during the filament fabrication, as well as during the 3D printing course, did not degrade or influence the thermal stability of PEEK, TGA (PerkinElmer Diamond TG/TDA, PerkinElmer, Inc., Waltham, Massachusetts, United States of America, heating cycle from 32 °C to 550 °C, heating step of 10 °C/min, a nitrogen atmosphere) was performed (Fig. 2a). The graph of weight loss (%) vs. temperature ($^{o}$C) verified the accomplishment of this goal.

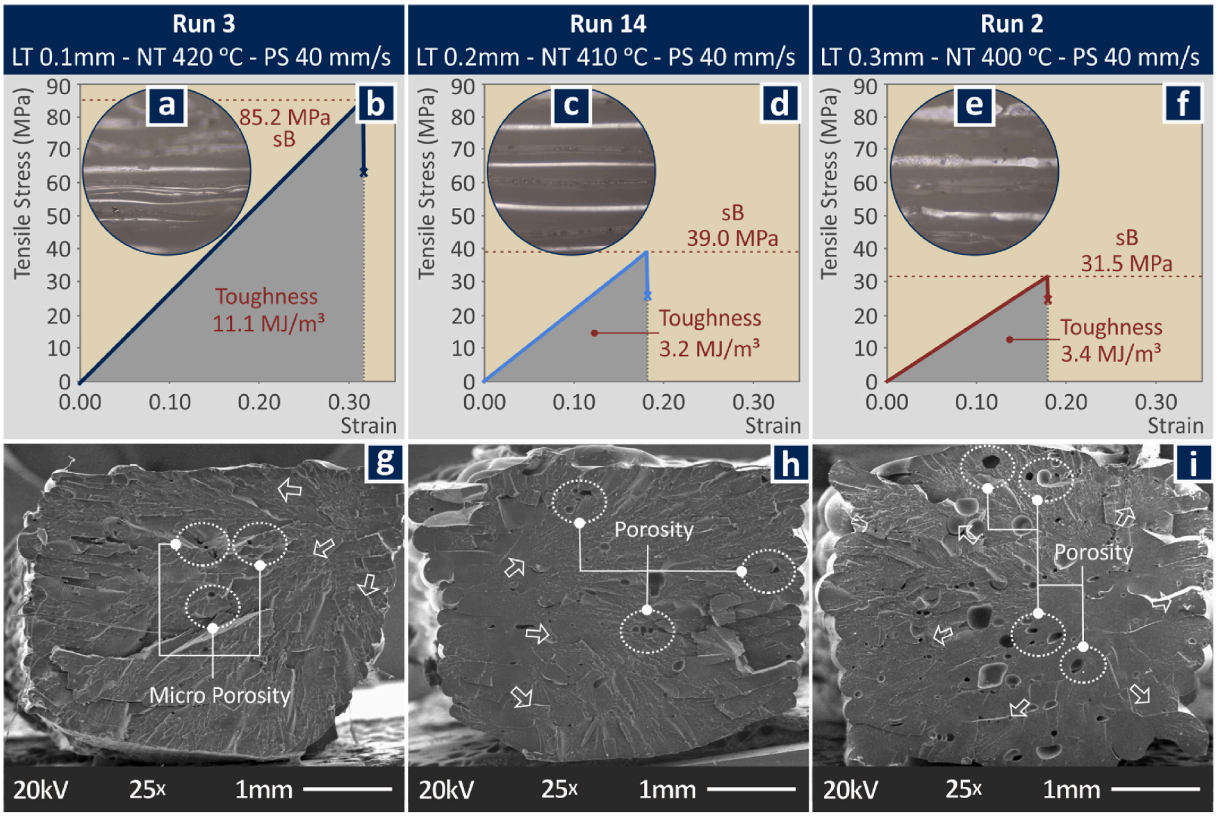


**Fig. 3.** For one randomly selected sample of run 3, run 14, and run 2, (a), (c), and (e) present SEM images from the side surface of the corresponding run, (b), (d), and (f) present tensile test results in stress vs strain graph form and (g), (h), and (i) present SEM images from the corresponding samples' fracture surfaces.

### 2.1. Energy indicators

The overall consumption of electric energy throughout the MEX-AM course consisted of three main components: e.g., (i) consumption during the startup of the machine, (ii) consumption during the productive 3D printing phase, and (iii) consumption during machine shutdown. Moreover, the total energy consumption was derived using the following equation (1) [9]:

$$E_{total} = E_{thermal} + E_{motion} + E_{auxiliary} \quad (1)$$

where $E_{thermal}$ is the thermal energy consumed, calculated by the following equation (2):

$$E_{thermal} = E_{heating} + E_{cooling} \quad (2)$$

$E_{motion}$ is the energy consumed by the feed motors of the 3D printing apparatus and $E_{auxiliary}$ is calculated by the following equation (3)

$$E_{auxiliary} = E_{startup} + E_{steady-state} + E_{shutdown} \quad (3)$$

And is defined as the energy consumed by the electronic circuits and the remaining subparts of the 3D printing device.
To generalize the energy documentation, the Specific Printing Energy metric is obtained using the following equation (4):

$$SPE = \frac{EPC}{w}\,[MJ / g] \quad (4)$$

whereas the Specific Printing Power metric derives from the following equation (5):

$$SPP = \frac{EPC}{PT \bullet w} \bullet 10^3\,[kW / g] \quad (5)$$

where Energy Printing Consumption (EPC) represents the energy used by the 3D printer ($E_{total}$), w is the actual weight of each specimen, and PT is the actual printing time for each experimental run.

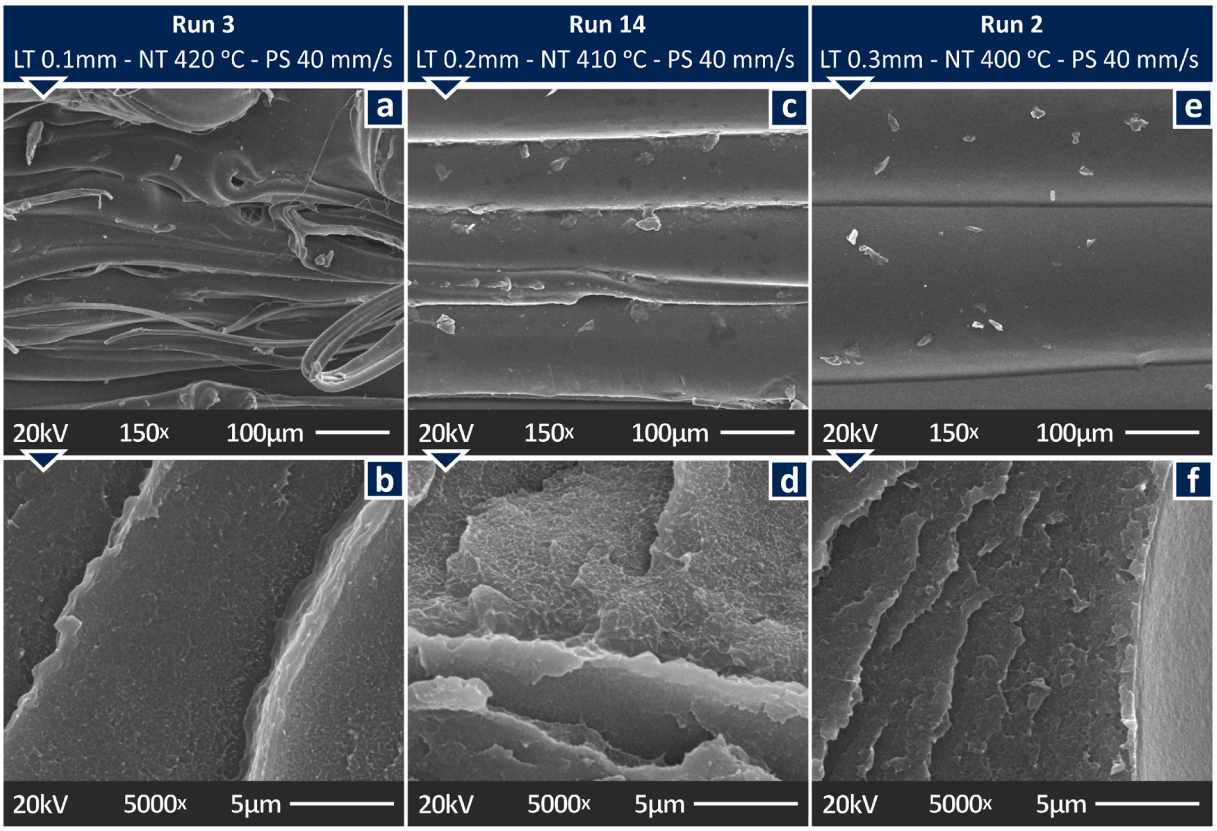


**Fig. 4.** SEM images from the side surface of a randomly selected sample of (a) run 3, (c) run 14, (e) run 2, and the corresponding fracture surface images of the samples (b) run 3, (d) run 14, (f) run 2. The conditions, that each run was built are depicted in the image.

### *2.2. Design of experiment, statistical analysis, and ANOVA*

Box–Behnken experimental design is frequently used for process optimization in 3D printing [53,60–63]. In the current study, this type of design was used for the optimization of the input parameters (3D printing settings) in terms of the tensile strength and energy consumption of parts made by MEX 3D printing with a high-performance PEEK polymer. Three input process parameters were selected: layer thickness, nozzle temperature, and printing speed. The process parameter levels were fixed (coded values: −1, 0, and 1), resulting in 15 experimental runs, which is an optimization approach that is commonly used in the literature [63,64]. The input parameters (3D printing settings) and their levels were chosen in accordance with the literature review. For instance, the literature reports nozzle temperature as the most critical parameter for 3D printing with the MEX process PEEK polymer [53]. To select the input parameter levels, the specifications of the PEEK polymer provided in its datasheet and 3D printer specifications were also considered. Overall, these specific 3D printing parameters were considered in the study for the reasons explained above and additionally because they have not been tested yet for the PEEK polymer, and literature on energy consumption on 3D printed parts suggests that they significantly affect energy consumption [65–67].

The experimental results were analyzed, and MEP and interaction plots were formed to identify the optimum parameters and the interaction between the input parameters. The regression followed and prediction models were compiled as functions of the input parameters, for the part weight (g), printing time (s), EPC (MJ), SPE (MJ/g), and SPP (kW/g) energy indicators, whereas for sB (MPa), E (MPa), and toughness (integral of the stress vs. strain curve produced in the tensile experiment) (MJ/m$^3$). The prediction quadratic equations were validated through an additional run for confirmation.

## 3. Results and discussion

### *3.1. Failure analysis and morphological characteristics*

Runs 3, 2, and 14 were selected for further analysis. The stress vs. strain diagrams for one randomly selected specimen out of five in each run are presented in Fig. 3b, d, and f respectively. The 3D printing settings used for each run are shown in Fig. 2b. These runs were selected to have different values for the two 3D printing parameters (LT and NT), and the same PS value, to present the differences more clearly between the cases studied. The corresponding tensile strength, sB (MPa), and toughness (MJ/m$^3$) values are shown in

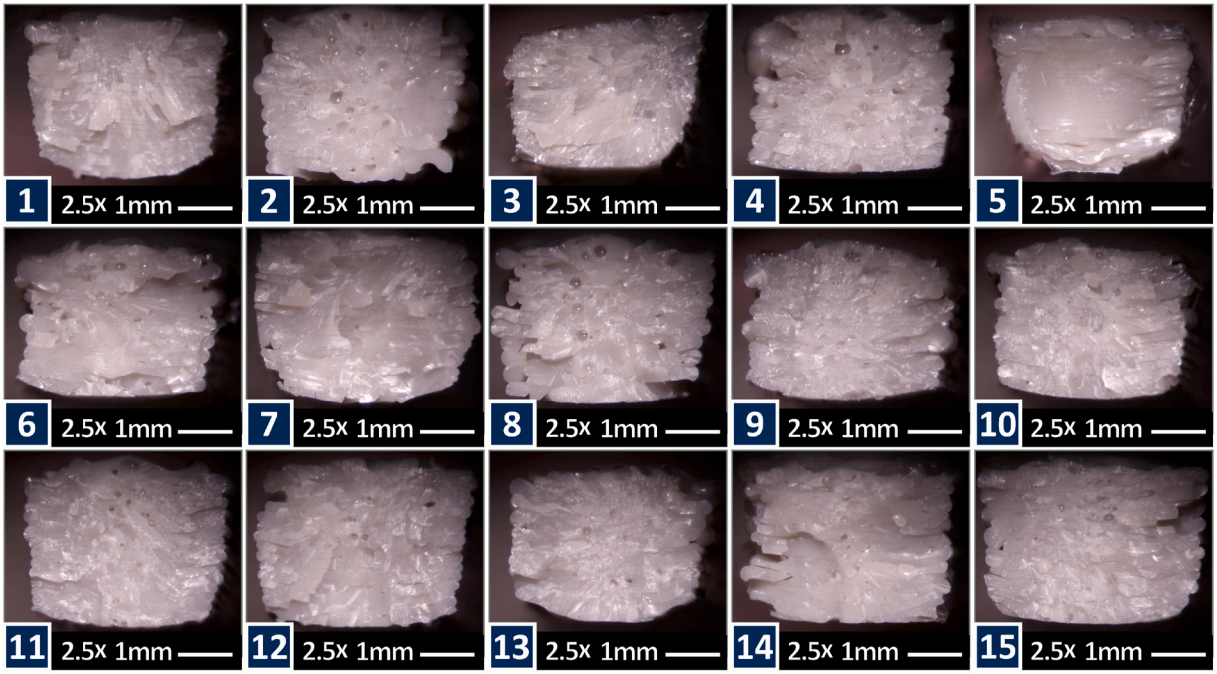


**Fig. 5.** Images from the stereoscope from the fracture surface of a randomly selected sample from each run (1–15, numbers in the images correspond to the respective run).

Fig. 3d, d, and f respectively, as mentioned. It should be noted that forces approximately up to 1000 N were applied in these samples in the experiments carried out within the context of the study.

Fig. 3a, c, and e present a stereoscopic image from the side surface of the corresponding sample. As shown, sB significantly differed between the cases studied, with run 2 (Fig. 3d) having 2.7 times lower strength than run 3 (Fig. 3b). This demonstrates the extent to which the 3D printing settings can affect the performance of the parts. The Run 3 sample can be evaluated as a high-performance polymer, while the strength of the sample in Run 2 is similar to that of commonly used polymers such as PLA [18]. The differences in the 3D printed structure are visible in the stereoscopic pictures (Fig. 3a, c, and e), especially with respect to the LT parameter. More uniform fusion was observed in runs 2 (Figs. 3e) and 14 (Fig. 3c); however, the mechanical strength was inferior to that of run 3 (Fig. 3a). Fig. 3 also presents SEM images of the fracture surfaces of the samples (Fig. 3g, h, and i, respectively, for the three runs). In all three runs, a brittle fracture mechanism was observed, with minimum deformation present on the fracture surface. In all the images, the arrows indicate an estimation of the evolution of the fracture on the surface. In run 3 (Fig. 3g), the fracture appeared to start from the top left vertex of the sample, in run 14 (Fig. 3h) from the left edge, as shown in the image, and for run 2 (Fig. 3i) in the middle of the specimen. The deformation was slightly higher in run 3 (Fig. 3g), and brittle failure still occurred. Porosity is visible on the fracture surface, which is expected because of the layer-by-layer 3D printing structure of the samples [68]. Through an optical inspection of the specimens, the porosity was found to be lower in the fracture surface of run 3 compared to that of run 14. On the other hand, a more extensive count and larger voids were visible in run 2. This agrees with the tensile test results, in which the sample from run 2 showed inferior mechanical properties, and the corresponding literature reports that increased porosity negatively affects the mechanical properties of the parts [69]. These findings agree with the literature on the fracture mechanisms of 3D printed parts, which have been thoroughly investigated and analyzed [70–78].

Fig. 4 shows the corresponding SEM images for the specific runs (and samples) mentioned above (runs 3, 14, and 2). SEM images were taken from the side surfaces of the samples, whereas higher-magnification images were taken from the fracture surfaces. From the side surface images, run 2 (Fig. 4e) shows defect-free layer fusion, so the inferior tensile strength can be attributed to the internal porosity of the specimens. In run 14 (Fig. 4c), voids were observed owing to the 3D printing process and the parameters used. Run 3 (Fig. 4a) showed a non-uniform shape layer structure with small voids and defects. Nevertheless, the tensile strength increased in the samples of this run (run 3) owing to the more solid internal structure with fewer pores and better adhesion between the strands. In the higher-magnification images of the fracture surfaces of the samples, the morphology observed is typical for polymeric materials [79–81], although differences can be observed between the specimens. Run 3 (Fig. 4b) showed a more uniform fracture pattern, and run 14 (Fig. 4d) had a rougher surface with high and low hills formed in the fracture area. Run 2 (Fig. 4f) also had a rather smooth pattern in the fracture area, but internal cracks could be observed in the image.

Fig. 5 shows images taken with a stereoscope of the entire fracture surface of one specimen from each of the 15 runs. Differences between the samples are evident, with some surfaces being rougher than others; some samples have a smoother fracture surface, for example, the sample from run no. 5 (Figs. 5–5), and in some samples, parts of the material have been abstracted, forming cavities on the surface, for example, in the sample from run 14 (Figs. 5–14). These differences indicate that different 3D printing settings affect the

**Table 2**
Box Behnken Design: Input Parameters, their Levels, Average Values, and Standard Deviations for metrics: Printing Time, Tensile Strength (sB), and the EPC.

| Run | LT (mm) | NT (°C) | PS (mm/min) | Weight (g) | Printing Time (s) | sB (MPa) | EPC (MJ) |
|---|---|---|---|---|---|---|---|
| 1 | 0.1 | 400 | 40 | 2.10 ± 0.02 | 1013.20 ± 37.41 | 81.67 ± 5.85 | 0.554 ± 0.037 |
| 2 | 0.3 | 400 | 40 | 2.16 ± 0.03 | 367.20 ± 21.43 | 32.04 ± 3.07 | 0.183 ± 0.005 |
| 3 | 0.1 | 420 | 40 | 2.08 ± 0.03 | 1016.00 ± 72.46 | 87.71 ± 6.55 | 0.603 ± 0.033 |
| 4 | 0.3 | 420 | 40 | 2.15 ± 0.03 | 380.60 ± 20.40 | 48.68 ± 3.52 | 0.142 ± 0.010 |
| 5 | 0.1 | 410 | 30 | 2.10 ± 0.04 | 1275.40 ± 85.39 | 82.51 ± 6.97 | 0.689 ± 0.047 |
| 6 | 0.3 | 410 | 30 | 2.07 ± 0.04 | 517.80 ± 22.62 | 29.43 ± 2.32 | 0.326 ± 0.032 |
| 7 | 0.1 | 410 | 50 | 2.03 ± 0.01 | 855.20 ± 14.04 | 42.33 ± 3.22 | 0.451 ± 0.027 |
| 8 | 0.3 | 410 | 50 | 2.16 ± 0.04 | 322.60 ± 27.19 | 53.75 ± 4.17 | 0.148 ± 0.008 |
| 9 | 0.2 | 400 | 30 | 2.10 ± 0.03 | 675.40 ± 32.39 | 47.22 ± 3.24 | 0.405 ± 0.014 |
| 10 | 0.2 | 420 | 30 | 2.14 ± 0.04 | 730.00 ± 17.32 | 49.73 ± 2.22 | 0.324 ± 0.024 |
| 11 | 0.2 | 400 | 50 | 2.14 ± 0.02 | 478.20 ± 19.28 | 35.47 ± 3.20 | 0.210 ± 0.020 |
| 12 | 0.2 | 420 | 50 | 2.08 ± 0.01 | 479.60 ± 28.59 | 60.05 ± 6.46 | 0.217 ± 0.024 |
| 13 | 0.2 | 410 | 40 | 2.14 ± 0.02 | 548.40 ± 37.10 | 39.99 ± 2.67 | 0.320 ± 0.024 |
| 14 | 0.2 | 410 | 40 | 2.10 ± 0.03 | 527.20 ± 21.14 | 41.34 ± 3.74 | 0.284 ± 0.023 |
| 15 | 0.2 | 410 | 40 | 2.14 ± 0.04 | 548.20 ± 30.15 | 42.24 ± 1.15 | 0.323 ± 0.032 |

**Table 3**
Average Values and Standard Deviations for metrics: SPE, SPP, Tensile Modulus of Elasticity (E), and Tensile Toughness.

| Run | SPE (MJ/g) | SPP (kW/g) | E (MPa) | Toughness (MJ/m$^3$) |
|---|---|---|---|---|
| 1 | 0.264 ± 0.018 | 0.261 ± 0.020 | 277.25 ± 7.61 | 10.53 ± 1.08 |
| 2 | 0.085 ± 0.003 | 0.231 ± 0.020 | 190.27 ± 4.28 | 3.04 ± 0.28 |
| 3 | 0.289 ± 0.014 | 0.287 ± 0.032 | 264.32 ± 6.36 | 12.26 ± 1.06 |
| 4 | 0.066 ± 0.005 | 0.173 ± 0.015 | 234.03 ± 5.11 | 5.16 ± 0.44 |
| 5 | 0.328 ± 0.027 | 0.258 ± 0.023 | 272.69 ± 7.99 | 12.88 ± 0.73 |
| 6 | 0.157 ± 0.015 | 0.304 ± 0.019 | 181.22 ± 3.44 | 2.51 ± 0.22 |
| 7 | 0.221 ± 0.012 | 0.259 ± 0.015 | 174.00 ± 5.44 | 5.12 ± 0.55 |
| 8 | 0.068 ± 0.005 | 0.212 ± 0.018 | 268.14 ± 10.00 | 5.00 ± 0.45 |
| 9 | 0.193 ± 0.007 | 0.286 ± 0.017 | 261.75 ± 4.06 | 4.49 ± 0.50 |
| 10 | 0.152 ± 0.013 | 0.208 ± 0.021 | 258.22 ± 6.27 | 4.71 ± 0.44 |
| 11 | 0.098 ± 0.010 | 0.205 ± 0.025 | 233.18 ± 7.52 | 2.84 ± 0.25 |
| 12 | 0.104 ± 0.011 | 0.219 ± 0.033 | 276.53 ± 3.67 | 6.27 ± 1.09 |
| 13 | 0.150 ± 0.011 | 0.274 ± 0.029 | 209.06 ± 5.95 | 4.57 ± 0.41 |
| 14 | 0.135 ± 0.009 | 0.257 ± 0.021 | 240.24 ± 6.59 | 3.90 ± 0.46 |
| 15 | 0.151 ± 0.017 | 0.277 ± 0.037 | 227.80 ± 8.65 | 3.26 ± 0.29 |

performance of the samples. Further analysis is required, employing modeling tools to quantitatively identify the impact rate of each control setting on the performance of the AM-made specimens. The descriptive analysis is as follows.

### 3.2. Box-Behnken experimental design

The Box-Behnken design with the input parameters, their levels, and the values for each input parameter in each run are listed in Table 2. Table 2 also presents the average value and deviation calculated for the five replicas of each run for four of the response parameters studied herein, that is, part weight (g), printing time (s), tensile strength (MPa), and EPC (MJ). Table 3 presents the corresponding experimental results for the remaining metrics explored in the current study: SPE (MJ/g), SPP (kW/g), E (MPa), and toughness (MJ/m$^3$). Metrics B, E, and toughness are responses related to the mechanical efficiency of the MEX 3D-printed parts, while the remaining ones correspond to the energy consumption and eco-friendliness of the MEX process when fabricating parts with the PEEK high-performance polymer.

### 3.3. Statistical analysis

Based on the experimental results above, box plots were formed for four response parameters, that is, printing time (s) (Fig. 6a), part weight (g) (Fig. 6b), tensile strength (MPa) (Fig. 6c), and EPC (MJ) (Fig. 6d), to identify which 3D printing parameters have a strong effect on each specific response parameters. The scatter response of the values for each 3D printing parameter shows the strong influence of this 3D printing parameter on the specific response parameter. For the printing time, the PS and NT values are gathered around three values, which is not a clear compact response; however, the points are not scattered throughout the range of the values. Scattered values are shown for the LT parameter for the 0.1 mm value. For the remaining LT values, the points are rather compact. For the part weight parameter, the points are scattered in all cases. Similar observations were made for the tensile strength and EPC values. This strong influence of the input parameters indicates that further analysis of the results is required to provide additional and more solid conclusions about the effect of the input parameters on each response parameter. In this direction, MEP and interaction plots were

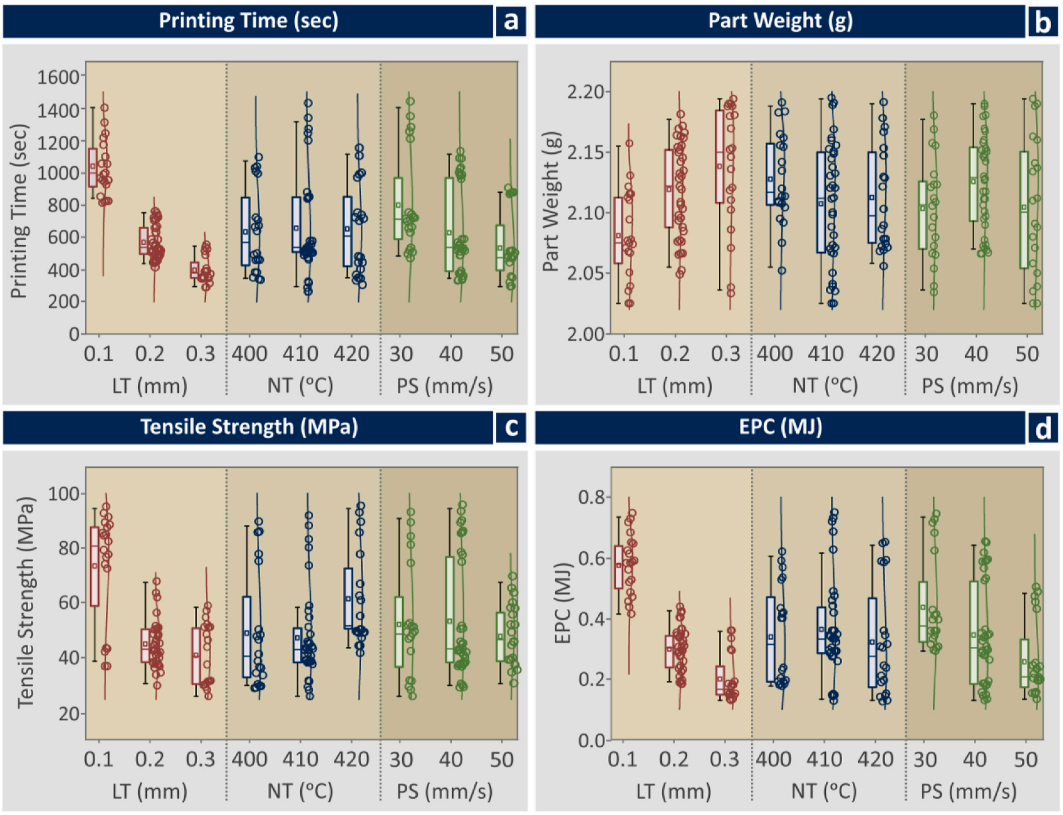


**Fig. 6.** Box plots for the main response metrics over the control parameters: (a) printing time (s), (b) part weight (g), (c) tensile strength (MPa), (d) EPC (MJ).

formed and are discussed further in Figs. 7–9.

The MEP for the response parameters of this work are presented in Fig. 7. An increase in LT decreases the printing time and increases the part weight. NT has a moderate effect on the printing time, whereas the weight of the part decreases with an increase in NT. The lowest part weight value was reported for the median NT value; however, the part weight was lower in the highest NT than in the lowest value tested. An increase in PS decreased the printing time. The lower and higher PS values reduced the weight of the part, whereas the median value increased the response parameter (Fig. 7a). An increase in LT decreased sB and EPC. The highest NT value increased sB, whereas NT had a moderate effect on EPC. High PS values reduced the EPC and sB values. The highest sB value was reported for a median PS of 40 mm/min (Fig. 7b). High LT values decrease the tensile modulus of elasticity. LT has a moderate effect on tensile toughness. A similar response was reported for NT regarding the modulus of elasticity and toughness. The median NT value reduced both response parameters and the highest values were reported for the highest NT at 420 °C considered in this study. Overall, PS had a moderate effect on both the modulus of elasticity and toughness metrics. Higher PS values slightly increased the tensile toughness, whereas the lowest PS value of 30 mm/min slightly increased the tensile modulus of elasticity (Fig. 7c). Higher LT and PS values decreased SPE and SPP. NT had a moderate effect on the SPE parameters. For the SPP parameter, the highest value was reported for the median NT parameter, and the lowest value was reported for the highest NT value (Fig. 7d).

Interaction plots of the input parameters for the printing time and part weight response parameters are presented in Fig. 8. More specifically, Fig. 8a presents for the printing time, the interactions between the control parameters LT and NT, Fig. 8b presents the corresponding interactions between LT and PS, and Fig. 8c presents the corresponding interactions between the NT and the PS control parameters. For the part weight response parameter, Fig. 8d presents the interactions between the control parameters LT and NT, Fig. 8e presents the corresponding interactions between LT and PS, and Fig. 8f presents the corresponding interactions between the NT and the PS control parameters. For the printing time, PS has an antagonistic relationship with NT, whereas all the other input parameter combinations show synergistic relations. For the part weight, all the input parameters show antagonistic relationships with each other. For the tensile strength response parameter, the interactions between the control parameters LT and NT, are depicted in Fig. 9a, while Fig. 9b presents the corresponding interactions between LT and PS, and Fig. 9c presents the corresponding interactions between the NT and the PS control parameters. For the EPC response parameter, Fig. 9d presents the interactions between the control parameters LT and NT, Fig. 9e presents the corresponding interactions between LT and PS, and Fig. 9f presents the corresponding interactions between the NT and the PS control parameters. LT showed a synergistic relationship with NT, and all the other input parameter combinations showed antagonistic behavior (Fig. 9). For the EPC response parameter, NT and PS showed antagonistic

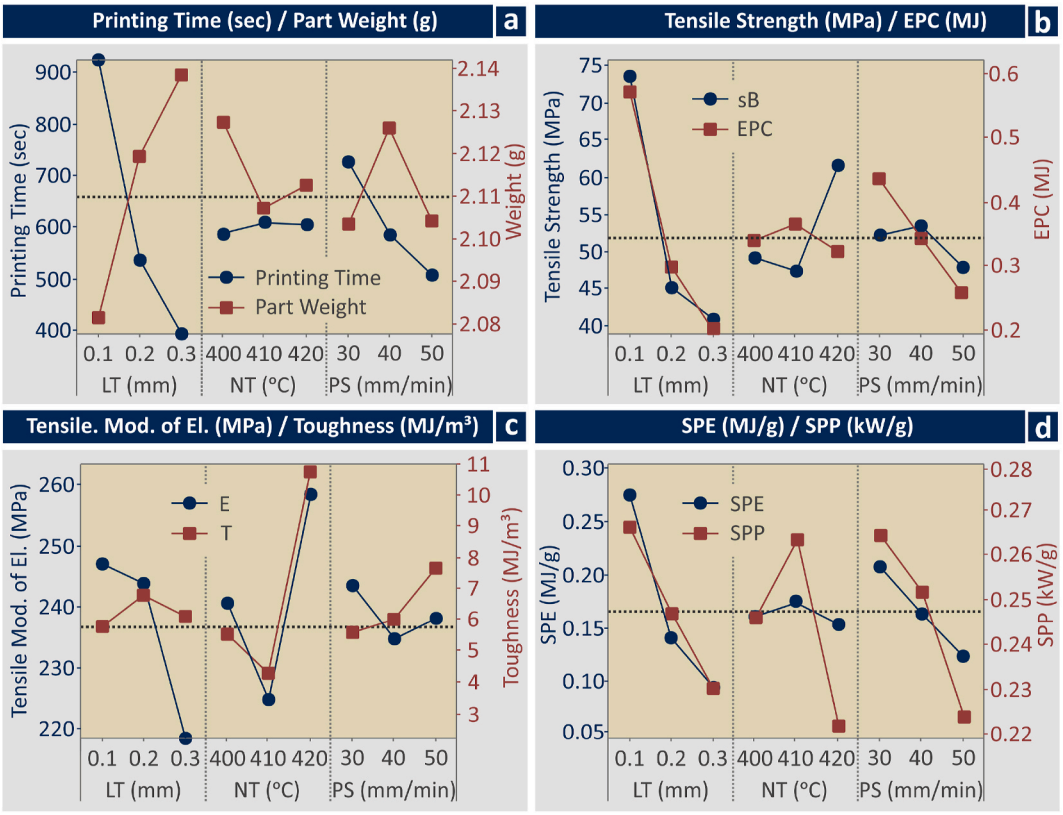


**Fig. 7.** MEP (a) printing time (s)/part weight (g), (b) tensile strength (MPa) over EPC (MJ), (c) Elasticity modulus (MPa) over toughness (MJ/m$^3$), (d) SPE (MJ/g) over SPP (kW/g).

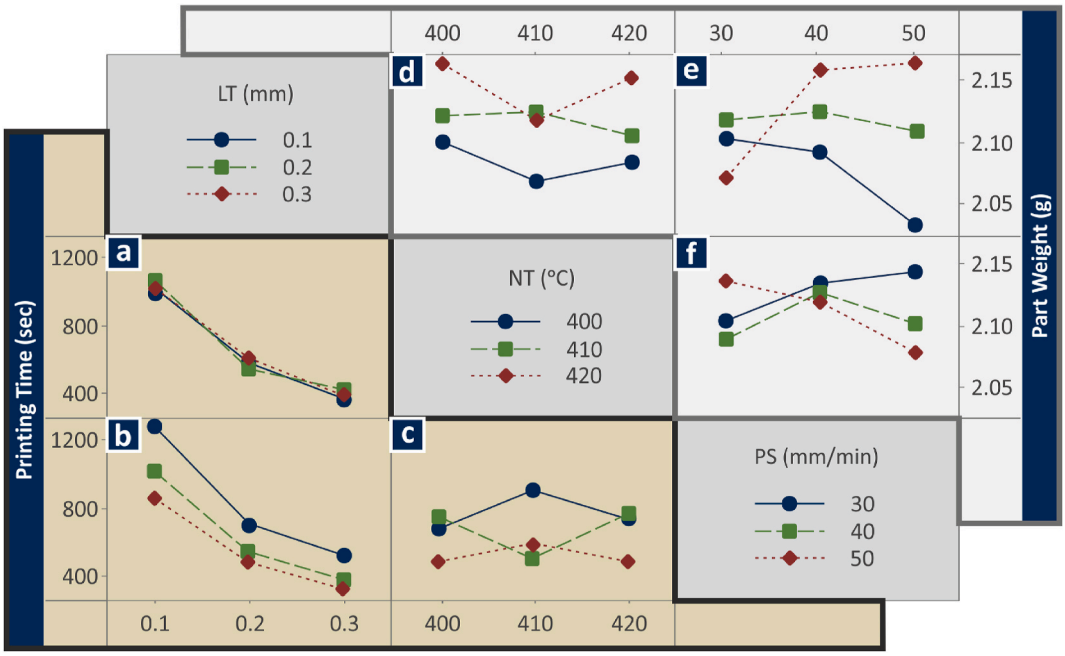


**Fig. 8.** Interaction plots printing time (s) (a) LT vs NT, (b) LT vs PS, (c) NT vs PS and part weight (g) (d) LT vs NT, (e) LT vs PS, and (f) NT vs PS.

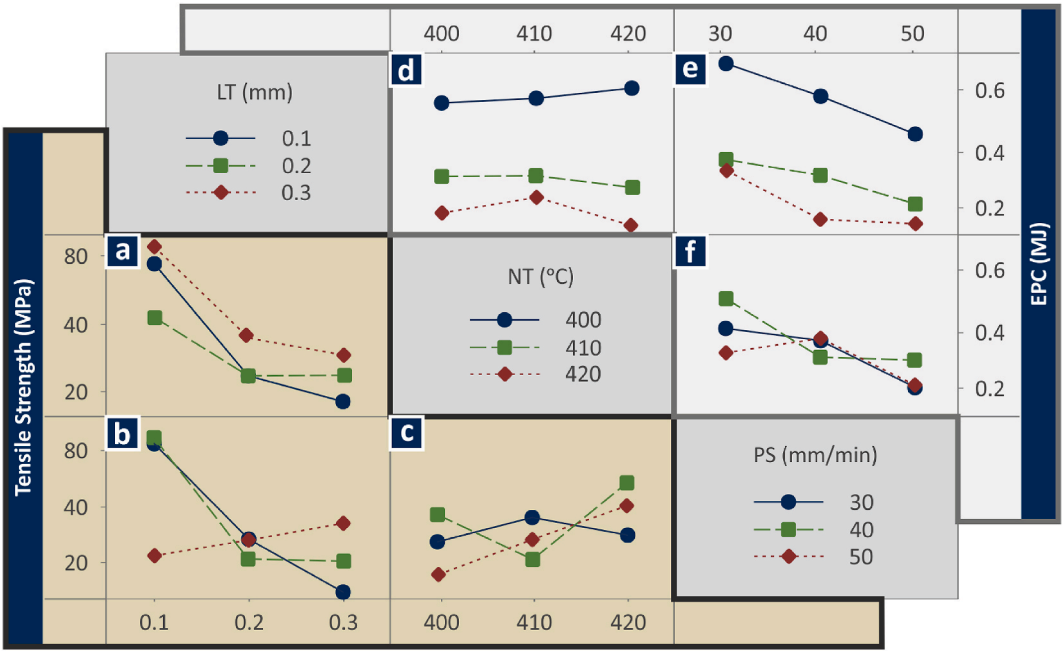


**Fig. 9.** Interaction plots tensile strength (MPa) (a) LT vs NT, (b) LT vs PS, (c) NT vs PS and EPC (MJ) (d) LT vs NT, (e) LT vs PS, and (f) NT vs PS.

behavior, and all the other input parameter combinations showed synergistic relations.

The challenge in this study was to produce parts with the high-performance PEEK polymer using the MEX 3D printing process, with optimized mechanical properties and consuming as little energy as possible. This is a critical task considering the overall eco-friendliness of the AM process and the high temperatures required to manufacture parts with MEX 3D printing using PEEK thermoplastics, which consequently leads to increased energy requirements. However, this was not possible. The analysis and optimization process indicated that either the energy consumption or mechanical strength could be optimized simultaneously.

From the literature review, the mechanical properties of MEX 3D printed PEEK samples and how they are affected by the 3D printed settings have been reported [27,43,82]. In Ref. [82] the same 3D printing parameters (NT, LT, and PS) were investigated, and the results were in agreement with the current work. Lower LT and high NT values resulted in better tensile strength. Regarding PS, in Ref. [82], a low PS of 20 mm/min achieved better mechanical properties. Such PS values were not studied herein; however, an increase in PS reduced the tensile strength. In the work of Sun Xiaoyong et al. [27] different 3D printing parameters were studied (bed temperature, ambient temperature, and filling ratio); therefore, the results cannot be directly correlated. In Ref. [43], LT and raster angle were investigated for their effect on the flexural and compressive strengths of PEEK 3D printed parts. Again, the results cannot be directly correlated; however, LT at higher values than the current work achieved the best mechanical performance. Such variations can be attributed to dissimilar PEEK grades, background conditions, and mainly to the different types of loading, in which the effect of LT is expected to differ. Previous research investigating the effect of nozzle diameter, nozzle temperature, and printing speed (two out of three factors under examination herein) on the flexural and compressive strengths of PEEK 3D fabricated parts [53] exploited the same experimental design for the analysis (Box-Behnken). In the same previous work, the nozzle diameter was the dominant parameter, followed by PS and NT. In the current work, PS was not as significant a parameter as in Ref. [53], whereas NT was a more important parameter affecting the results. In addition, such variances can be attributed mainly to the different types of experimental testing (compression and flexural tests) among other factors, as mentioned above.

However, the energy consumption when 3D printing parts with the PEEK polymer has not yet been presented in the literature, so the results of this work cannot be correlated with the literature. In a study on the energy consumption of MEX 3D printed ABS parts [9], the results were in good agreement with the outcomes of the current research. The increase in PS and LT decreases the energy consumption but has a negative effect on the mechanical strength of the specimens, which is the same finding as the current work for the PEEK polymer. Overall, the outcomes of the analysis, interactions, and effects of the 3D printing control settings on the studied indices showed that the approach followed was necessary, as such interpretation was not possible otherwise.

### *3.4. Regression analysis and ANOVA*

The full Quadratic Regression Model (QRM) for the response metrics is compiled as presented in the following equation (6):

$$Y_k = a_{i,k} + \sum_{i=1}^{n} b_{i,k}x_i + \sum_{i=1}^{n} c_{i,k}x_i^2 + \sum_{i}\sum_{j} d_{ij,k}x_i x_j + e_k \quad (6)$$

**Table 4**
Polynomial ANOVA, Specimen Weight vs LT, NT, PS.

| Source | DF | Adj SS | Adj MS | F-Value | *P*-Value |
|---|---|---|---|---|---|
| Regression | 9 | 0.092170 | 0.010241 | 11.34 | 0.000 |
| LT | 1 | 0.000245 | 0.000245 | 0.27 | 0.604 |
| NT | 1 | 0.001630 | 0.001630 | 1.81 | 0.184 |
| PS | 1 | 0.013122 | 0.013122 | 14.54 | 0.000 |
| $LT^2$ | 1 | 0.001940 | 0.001940 | 2.15 | 0.148 |
| $NT^2$ | 1 | 0.002016 | 0.002016 | 2.23 | 0.140 |
| $PS^2$ | 1 | 0.008653 | 0.008653 | 9.59 | 0.003 |
| LT × NT | 1 | 0.000034 | 0.000034 | 0.04 | 0.847 |
| LT × PS | 1 | 0.032482 | 0.032482 | 35.98 | 0.000 |
| NT × PS | 1 | 0.011424 | 0.011424 | 12.66 | 0.001 |
| Error | 65 | 0.058678 | 0.000903 | | |
| Total | 74 | 0.150848 | 0.011144 | | |
| $R^2$ | 61.10% | | | | |
| $R^2$ (adj) | 55.72% | | | | |
| $R^2$ (pred) | 48.64% | | | | |

**Table 5**
Polynomial ANOVA, Printing Time vs LT, NT, PS.

| Source | DF | Adj SS | Adj MS | F-Value | *P*-Value |
|---|---|---|---|---|---|
| Regression | 9 | 5368227 | 596470 | 364.86 | 0.000 |
| LT | 1 | 18662 | 18662 | 11.42 | 0.001 |
| NT | 1 | 1 | 1 | 0.00 | 0.985 |
| PS | 1 | 97 | 97 | 0.06 | 0.808 |
| $LT^2$ | 1 | 429158 | 429158 | 262.52 | 0.000 |
| $NT^2$ | 1 | 5 | 5 | 0.00 | 0.956 |
| $PS^2$ | 1 | 44356 | 44356 | 27.13 | 0.000 |
| LT × NT | 1 | 140 | 140 | 0.09 | 0.770 |
| LT × PS | 1 | 63281 | 63281 | 38.71 | 0.000 |
| NT × PS | 1 | 3538 | 3538 | 2.16 | 0.146 |
| Error | 65 | 106261 | 1635 | | |
| Total | 74 | 5474488 | 598105 | | |
| $R^2$ | 98.06% | | | | |
| $R^2$ (adj) | 97.79% | | | | |
| $R^2$ (pred) | 97.37% | | | | |

**Table 6**
Polynomial ANOVA, EPC vs LT, NT, PS.

| Source | DF | Adj SS | Adj MS | F-Value | *P*-Value |
|---|---|---|---|---|---|
| Regression | 9 | 1.91913 | 0.213236 | 181.96 | 0.000 |
| LT | 1 | 0.00122 | 0.001220 | 1.04 | 0.311 |
| NT | 1 | 0.01231 | 0.012309 | 10.50 | 0.002 |
| PS | 1 | 0.01324 | 0.013239 | 11.30 | 0.001 |
| $LT^2$ | 1 | 0.14293 | 0.142934 | 121.97 | 0.000 |
| $NT^2$ | 1 | 0.01295 | 0.012955 | 11.05 | 0.001 |
| $PS^2$ | 1 | 0.00073 | 0.000726 | 0.62 | 0.434 |
| LT × NT | 1 | 0.01012 | 0.010125 | 8.64 | 0.005 |
| LT × PS | 1 | 0.00446 | 0.004464 | 3.81 | 0.055 |
| NT × PS | 1 | 0.00980 | 0.009804 | 8.37 | 0.005 |
| Error | 65 | 0.07617 | 0.001172 | | |
| Total | 74 | 1.99530 | 0.214408 | | |
| $R^2$ | 96.18% | | | | |
| $R^2$ (adj) | 95.65% | | | | |
| $R^2$ (pred) | 94.87% | | | | |

where k is the response of a specific response output (e.g., Specimen Weight, Printing Time, sB, EPC, SPE, SPP, E, Toughness), a is the constant of the equation, b refers to the coefficients of the linear terms, c corresponds to the coefficients of the square terms, d represents the coefficients of the cross-product terms, e is the error (modeling residuals), and $x_i$ is the three (n = 3) control parameters, that is, the Layer Thickness, Nozzle Temperature, and Printing Speed.

The regression tables are presented (Tables 4–7). The regression tables for the remaining response indicators are presented in the Supplementary Material. The predictive models as a function of the three input parameters for each response indicator are also

**Table 7**
Polynomial ANOVA, sB vs LT, NT, PS.

| Source | DF | Adj SS | Adj MS | F-Value | *P*-Value |
|---|---|---|---|---|---|
| Regression | 9 | 22558.5 | 2506.50 | 62.22 | 0.000 |
| LT | 1 | 671.0 | 670.99 | 16.66 | 0.000 |
| NT | 1 | 1485.1 | 1485.08 | 36.87 | 0.000 |
| PS | 1 | 691.6 | 691.63 | 17.17 | 0.000 |
| $LT^2$ | 1 | 2936.2 | 2936.20 | 72.89 | 0.000 |
| $NT^2$ | 1 | 1404.9 | 1404.94 | 34.88 | 0.000 |
| $PS^2$ | 1 | 59.4 | 59.42 | 1.48 | 0.229 |
| LT × NT | 1 | 140.4 | 140.38 | 3.48 | 0.066 |
| LT × PS | 1 | 5200.0 | 5199.98 | 129.09 | 0.000 |
| NT × PS | 1 | 609.2 | 609.22 | 15.12 | 0.000 |
| Error | 65 | 2618.4 | 40.28 | | |
| Total | 74 | 25176.9 | 2546.78 | | |
| $R^2$ | 89.60% | | | | |
| $R^2$ (adj) | 88.16% | | | | |
| $R^2$ (pred) | 85.70% | | | | |

presented below (Equation (7)–(14)). In all tables, the F, p, and R values show regression accuracy. F values should be higher than four (4), p values should be lower than 0.05, and R values indicate the expected % accuracy of the prediction model. All response parameters satisfy the criteria for F and the p-value. The regression values for all the response parameters were close to or higher than 90%, which is an excellent result. Only in the case of the printing time, and regression values higher than 48.64% are expected for the SPP response indicator regression values higher than 50.55% are expected. For these two response metrics, the accuracy of the prediction models was expected to be lower. For the remaining metrics examined herein, associated with the mechanical strength metrics and energy consumption during the MEX 3D printing process of PEEK samples, the prediction models are more than adequate to provide accurate results.

$$Weight = 1.61 \times 10^{1} - 1.45 \times LT - 7.72 \times 10^{-2} \times NT + 1.07 \times 10^{-1} \times PS - 1.02 \times LT^{2} + 1.04 \times 10^{-4} \times NT^{2} - 2.16 \times 10^{-4} \times PS^{2} + 1.30 \times 10^{-3} \times LT \times NT + 4.03 \times 10^{-2} \times LT \times PS - 2.39 \times 10^{-4} \times NT \times PS \quad (7)$$

$$PrintingTime = 2.09 \times 10^{3} - 1.26 \times 10^{4} \times LT + 1.45 \times NT - 9.22 \times PS + 1.52 \times 10^{4} \times LT^{2} + 5.16 \times 10^{-3} \times NT^{2} + 4.90 \times 10^{-1} \times PS^{2} + 2.65 \times LT \times NT + 5.62 \times 10^{1} \times LT \times PS - 1.33 \times 10^{-1} \times NT \times PS \quad (8)$$

$$EPC = -4.08 \times 10^{1} + 3.23 \times LT + 2.12 \times 10^{-1} \times NT - 1.07 \times 10^{-1} \times PS + 8.79 \times LT^{2} - 2.64 \times 10^{-4} \times NT^{2} + 6.27 \times 10^{-5} \times PS^{2} - 2.25 \times 10^{-2} \times LT \times NT + 1.49 \times 10^{-2} \times LT \times PS + 2.21 \times 10^{-4} \times NT \times PS \quad (9)$$

$$sB = 1.57 \times 10^{4} - 2.39 \times 10^{3} \times LT - 7.36 \times 10^{1} \times NT - 2.46 \times 10^{1} \times PS + 1.26 \times 10^{3} \times LT^{2} + 8.72 \times 10^{-2} \times NT^{2} - 1.79 \times 10^{-2} \times PS^{2} + 2.64 \times LT \times NT + 1.61 \times 10^{1} \times LT \times PS + 5.51 \times 10^{-2} \times NT \times PS \quad (10)$$

$$E = 4.47 \times 10^{4} - 7.45 \times 10^{3} \times LT - 2.08 \times 10^{2} \times NT - 6.33 \times 10^{1} \times PS - 8.82 \times 10^{2} \times LT^{2} + 2.45 \times 10^{-1} \times NT^{2} + 7.13 \times 10^{-2} \times PS^{2} + 1.41 \times 10^{1} \times LT \times NT + 4.64 \times 10^{1} \times LT \times PS + 1.17 \times 10^{-1} \times NT \times PS \quad (11)$$

$$Toughness = 1.85 \times 10^{3} - 2.87 \times 10^{2} \times LT - 8.59 \times NT - 3.57 \times PS + 2.82 \times 10^{2} \times LT^{2} + 1.01 \times 10^{-2} \times NT^{2} - 3.54 \times 10^{-3} \times PS^{2} + 9.80 \times 10^{-2} \times LT \times NT + 2.56 \times LT \times PS + 8.01 \times 10^{-3} \times NT \times PS \quad (12)$$

$$SPE = -2.03 \times 10^{1} + 1.70 \times LT + 1.05 \times 10^{-1} \times NT - 5.72 \times 10^{-2} \times PS + 4.37 \times LT^{2} - 1.32 \times 10^{-4} \times NT^{2} + 4.58 \times 10^{-5} \times PS^{2} - 1.10 \times 10^{-2} \times LT \times NT + 4.31 \times 10^{-3} \times LT \times PS + 1.18 \times 10^{-4} \times NT \times PS \quad (13)$$

$$SPP = -4.78 \times 10^{1} + 9.36 \times LT + 2.39 \times 10^{-1} \times NT - 8.28 \times 10^{-2} \times PS - 1.37 \times 10^{-1} \times LT^{2} - 2.99 \times 10^{-4} \times NT^{2} - 9.76 \times 10^{-5} \times PS^{2} - 2.08 \times 10^{-2} \times LT \times NT - 2.31 \times 10^{-2} \times LT \times PS + 2.27 \times 10^{-4} \times NT \times PS \quad (14)$$

To further specify which parameters are statistically important in this study, Pareto charts were formed (Figs. 10 and 11). The

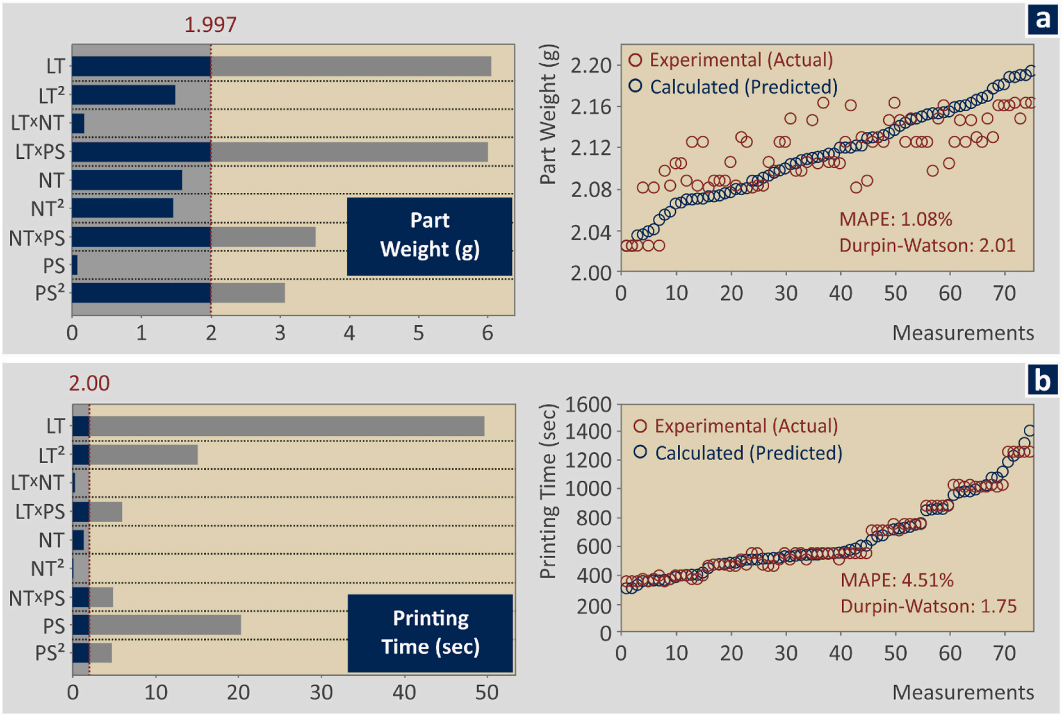


**Fig. 10.** Pareto and actual vs predicted graphs: (a) part weight (g), and (b) printing time (s).

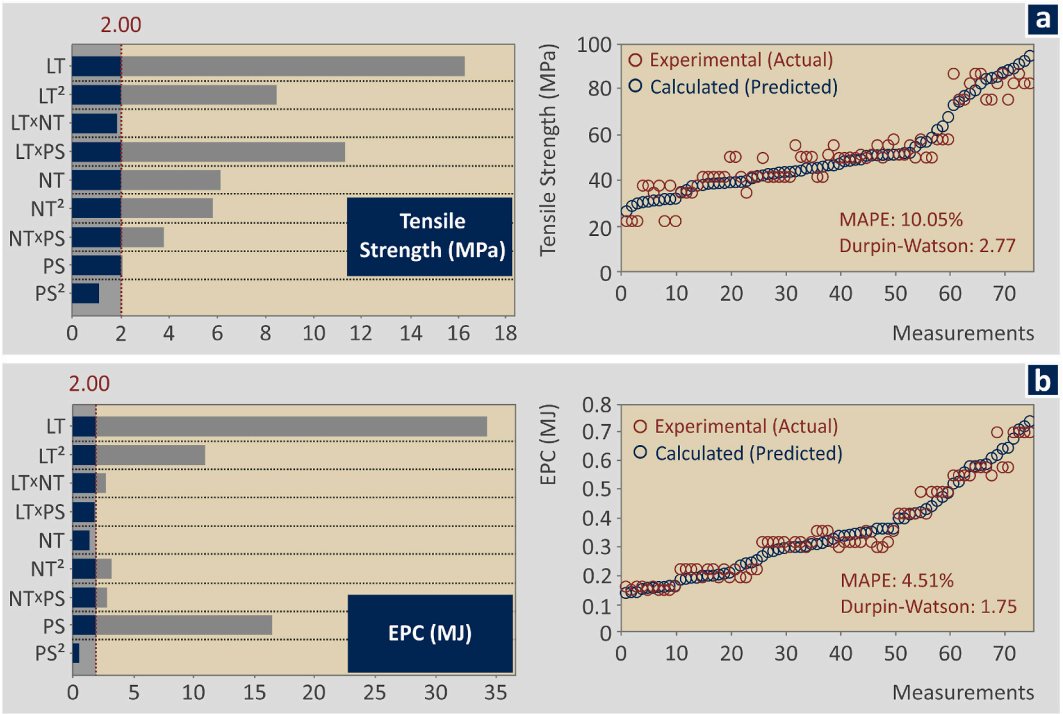


**Fig. 11.** Pareto and actual vs predicted graphs (a) tensile strength (MPa) and (b) EPC (MJ).

parameters that crossed the margin for each response parameter were statistically important for the specific response parameter. Next, an experimental vs. calculated graph (values derived from the respective prediction model) is presented. Two indicators were calculated and depicted in each graph: the Mean Absolute Percentage Error (MAPE) [83] (acceptable values regarding the prediction

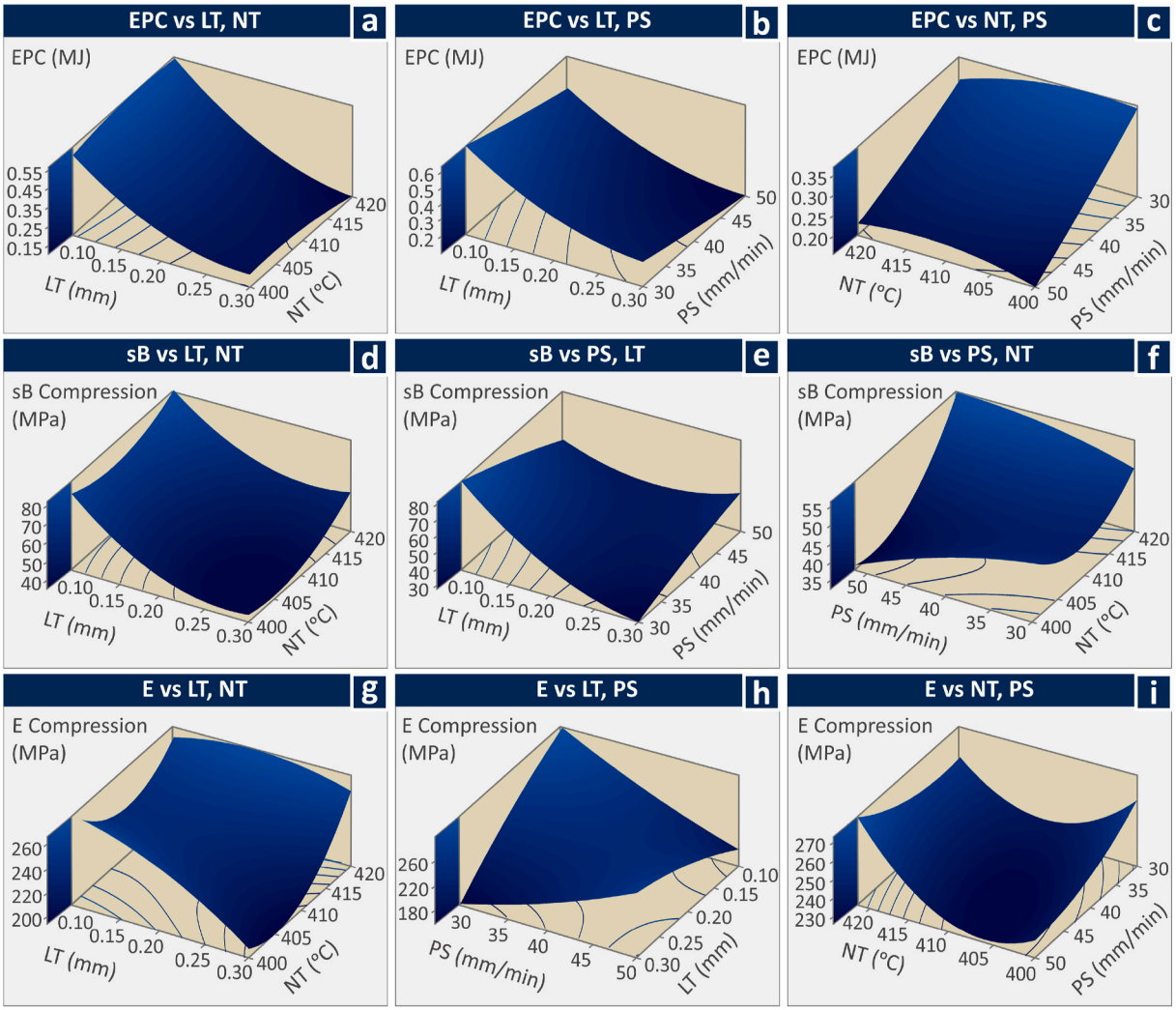


**Fig. 12.** Surface plots for (a), (b), (c) EPC (MJ), (d), (e), (f), sB and E (MPa) (g), (h), (i), vs the higher-ranked control parameters for each response parameter.

accuracy are the values that are lower than 5) and the Durbin-Watson statistic, which is an autocorrelation test of the regression results for each response parameter. A Durbin-Watson value of 2.0 shows zero (0) autocorrelation, higher values show negative autocorrelation and lower values show positive autocorrelation. In all charts, the MAPE value was acceptable, except for the tensile strength metric (MAPE 10.05% is reported). For part weight (Fig. 10a), LT, LT × PS, NT × PS, and $PS^2$ are statistically important parameters. The Durbin-Watson value showed a negative autocorrelation of the results. For the printing time (Fig. 10b), LT, $LT^2$, NT × PS, PS, and $PS^2$ were statistically important parameters. The Durbin-Watson value showed positive autocorrelation of the results. For the tensile strength (Fig. 11a), LT, $LT^2$, NT, $NT^2$, and PS were statistically important parameters. The Durbin-Watson value showed a negative autocorrelation of the results. For the EPC (Fig. 11b), LT, $LT^2$, NT × PS, $NT^2$, and PS were statistically important parameters. The Durbin-Watson value showed positive autocorrelation of the results. Finally, three-dimensional surface graphs were formed for the sB, E, and EPC response parameters versus the most critical input parameters for each of them (Fig. 12). More specifically, Fig. 12a, b, and c present a three-dimensional surface graph for the EPC metric versus the LT and the NT, the LT and the PS, and NT and the PS control parameters respectively. Fig. 12d, e, and f present a three-dimensional surface graph for the sB metric versus the LT and the NT, the PS and the LT, and PS and the NT control parameters respectively. Finally, Fig. 12g, h, and i present a three-dimensional surface graph for the E metric versus the LT and the NT, the LT and the PS, and NT and the PS control parameters respectively. Additional data regarding the analysis can be found in the supplementary material.

### *3.4. Confirmation experiments*

To evaluate the accuracy of the prediction models, an additional confirmation run (run 16) was conducted, with five replicates. The

**Table 8**
Control Parameters, their Levels and Average Values, and Standard Deviations of measured Response metrics for the Specimen Weight, Printing Time, Tensile Strength (sB), and the EPC for the Confirmation Run.

| Run | LT (mm) | NT (°C) | PS (mm/min) | Weight (g) | Printing Time (s) | sB (MPa) | EPC (MJ) |
|---|---|---|---|---|---|---|---|
| 16 | 0.1 | 400 | 30 | 2.20 ± 0.09 | 1305.00 ± 62.04 | 82.19 ± 7.04 | 0.634 ± 0.014 |

**Table 9**
Average Values and Standard Deviations of experimentally derived Responses for SPE, SPP, Tensile Modulus of Elasticity (E), and Tensile Toughness for the Confirmation Run.

| Run | SPE (MJ/g) | SPP (kW/g) | E (MPa) | Toughness (MJ/m$^3$) |
|---|---|---|---|---|
| 16 | 0.288 ± 0.012 | 0.221 ± 0.017 | 266.84 ± 9.13 | 11.53 ± 1.50 |

**Table 10**
Validation results.

| Run | | 16 |
|---|---|---|
| Actual | Weight (g) | 2.20 |
| | Printing Time (s) | 1305.00 |
| | EPC (MJ) | 0.63 |
| | SPE (MJ/g) | 0.29 |
| | SPP (kW/g) | 0.22 |
| | sB (MPa) | 82.19 |
| | E (MPa) | 266.84 |
| | Toughness (MJ/m$^3$) | 11.53 |
| Predicted | Weight (g) | 2.1138 |
| | Printing Time (s) | 1233.92 |
| | EPC (MJ) | 0.65104 |
| | SPE (MJ/g) | 0.32953 |
| | SPP (kW/g) | 0.25168 |
| | sB (MPa) | 97.46 |
| | E (MPa) | 329.57 |
| | Toughness (MJ/m$^3$) | 13.696 |
| Absolute Error | Weight (%) | 4.05 |
| | Printing Time (%) | 5.45 |
| | EPC (%) | 2.65 |
| | SPE (%) | 14.32 |
| | SPP (%) | 13.65 |
| | sB (%) | 18.58 |
| | E (%) | 23.51 |
| | Toughness (%) | 18.77 |

input parameter levels, along with the average values and standard deviations of the main response properties, are listed in Tables 8 and 9. Table 10 lists the actual values derived experimentally, the predicted values with the modeling equations for the response parameters, and the error between them. In all cases, the error was within acceptable limits, thereby verifying the reliability of the prediction models formed in the regression analysis. Only in the case of sB and E is the error slightly higher (approximately 20%), which is still an acceptable result, considering all the other metrics derived during the regression analysis for the accuracy of the prediction models. Such errors can be attributed to the values of the input parameters in the confirmation run, as the prediction models operate within limits in the range of the input parameters and their accuracy is not constant within these limits.

## 4. Conclusions

The research presented herein investigated three critical 3D printing parameters, that is, layer thickness, nozzle temperature, and printing speed, for their effect on the energy efficiency during the MEX 3D printing of parts made with high-performance PEEK thermoplastic. The impact of these three 3D printer settings on the mechanical strength scores of the PEEK MEX 3D printed parts in the tensile test was also evaluated in an attempt to build parts with optimized mechanical performance and reduced energy demands in the manufacturing process. This is critical considering the high temperatures required for the 3D printing of PEEK thermoplastics, which is expected to increase the required energy of the process and negatively impact its eco-friendliness. A Box–Behnken design was employed to achieve this goal. LT was the dominant parameter in terms of tensile strength and EPC. A higher sB was achieved (~74 MPa) with a lower LT of 0.1 mm, which had a negative effect on energy consumption. It was increased to ~0.58 MJ, while EPC as low as ~0.2 MJ was achieved in the study with an LT of 0.3 mm (290% higher EPC). Therefore, it was not possible to optimize both the energy consumption and tensile strength. According to the requirements of each application, either the mechanical properties or energy consumption can be optimized, and the predicted models can provide an estimation of the other response parameter values. The

credibility of the prediction models was verified using a confirmation run. The governing equations were shown to be satisfactory for predicting the response parameters studied herein, making them suitable for use in real applications. In future investigations, different or additional input parameters can be assessed, the levels of input settings can be further extended, and different experimental designs can be examined.

## Funding

This study received no external funding.

## Declaration of competing interest

The authors declare that they have no known competing financial interests or personal relationships that could have appeared to influence the work reported in this paper.

## Appendix A. Supplementary data

Supplementary data to this article can be found online at https://doi.org/10.1016/j.heliyon.2023.e18363.

## References

[1] T. Peng, K. Kellens, R. Tang, C. Chen, G. Chen, Sustainability of additive manufacturing: an overview on its energy demand and environmental impact, Addit. Manuf. 21 (2018) 694–704, https://doi.org/10.1016/j.addma.2018.04.022.
[2] M. Javaid, A. Haleem, R.P. Singh, R. Suman, S. Rab, Role of additive manufacturing applications towards environmental sustainability, Adv. Ind. Eng. Polym. Res. 4 (2021) 312–322, https://doi.org/10.1016/j.aiepr.2021.07.005.
[3] H.A. Colorado, E.I.G. Velásquez, S.N. Monteiro, Sustainability of additive manufacturing: the circular economy of materials and environmental perspectives, J. Mater. Res. Technol. 9 (2020) 8221–8234, https://doi.org/10.1016/j.jmrt.2020.04.062.
[4] V. Annibaldi, M. Rotilio, Energy consumption consideration of 3D printing, 2019 IEEE Int. Work. Metrol. Ind. 4.0 IoT, MetroInd 4.0 IoT 2019 - Proc (2019) 243–248, https://doi.org/10.1109/METROI4.2019.8792856.
[5] T. Peng, Analysis of energy utilization in 3D printing processes, Procedia CIRP 40 (2016) 62–67, https://doi.org/10.1016/j.procir.2016.01.055.
[6] M.R. Khosravani, T. Reinicke, On the environmental impacts of 3D printing technology, Appl. Mater. Today 20 (2020), 100689, https://doi.org/10.1016/j.apmt.2020.100689.
[7] T. Peng, W. Sun, Energy modelling for FDM 3D printing from a life cycle perspective, Int. J. Manuf. Res. 11 (2017) 1, https://doi.org/10.1504/ijmr.2017.10003722.
[8] M.A. El youbi El idrissi, L. Laaouina, A. Jeghal, H. Tairi, M. Zaki, Energy consumption prediction for fused deposition modelling 3D printing using machine learning, Appl. Syst. Innov. 5 (2022) 1–16, https://doi.org/10.3390/asi5040086.
[9] N. Vidakis, J.D. Kechagias, M. Petousis, F. Vakouftsi, N. Mountakis, The effects of FFF 3D printing parameters on energy consumption, Mater. Manuf. Process. 00 (2022) 1–18, https://doi.org/10.1080/10426914.2022.2105882.
[10] A. Dey, I.N. Roan Eagle, N. Yodo, I.N.R. Eagle, N. Yodo, I.N. Roan Eagle, N. Yodo, A review on filament materials for fused filament fabrication, J. Manuf. Mater. Process. 5 (2021), https://doi.org/10.3390/jmmp5030069.
[11] J. Kechagias, D. Chaidas, N. Vidakis, K. Salonitis, N.M.M. Vaxevanidis, Key parameters controlling surface quality and dimensional accuracy: a critical review of FFF process, Mater. Manuf. Process. 37 (2022) 963–984, https://doi.org/10.1080/10426914.2022.2032144.
[12] I. Jasiuk, D.W. Abueidda, C. Kozuch, S. Pang, F.Y. Su, J. McKittrick, An overview on additive manufacturing of polymers, JOM 70 (2018) 275–283, https://doi.org/10.1007/s11837-017-2730-y.
[13] N. Vidakis, M. Petousis, A. Maniadi, E. Koudoumas, A. Vairis, J. Kechagias, Sustainable additive manufacturing: mechanical response of acrylonitrile-butadiene-styrene over multiple recycling processes, Sustain. Times 12 (2020) 3568, https://doi.org/10.3390/su12093568.
[14] N. Vidakis, C. David, M. Petousis, D. Sagris, N. Mountakis, A. Moutsopoulou, The effect of six key process control parameters on the surface roughness , dimensional accuracy , and porosity in material extrusion 3D printing of polylactic acid : prediction models and optimization supported by robust design analysis, Adv. Ind. Manuf. Eng. 5 (2022), 100104, https://doi.org/10.1016/j.aime.2022.100104.
[15] A. Vairis, M. Petousis, N. Vidakis, K. Savvakis, On the strain rate sensitivity of Abs and Abs plus fused deposition modeling parts, J. Mater. Eng. Perform. 25 (2016) 3558–3565, https://doi.org/10.1007/s11665-016-2198-x.
[16] F. Saenz, C. Otarola, K. Valladares, J. Rojas, Influence of 3D printing settings on mechanical properties of ABS at room temperature and 77 K, Addit, Manuf 39 (2021), 101841, https://doi.org/10.1016/j.addma.2021.101841.
[17] M. Petousis, N. Vidakis, N. Mountakis, V. Papadakis, L. Tzounis, Three-dimensional printed polyamide 12 (PA12) and polylactic acid (PLA) Alumina (Al 2 O 3) nanocomposites with significantly enhanced tensile, Flexural , and Impact Properties (2022) 12.
[18] M. Petousis, N. Vidakis, N. Mountakis, V. Papadakis, S. Kanellopoulou, A. Gaganatsiou, N. Stefanoudakis, J. Kechagias, Multifunctional material extrusion 3D-printed Antibacterial polylactic acid (PLA) with binary inclusions: the effect of cuprous oxide and cellulose nanofibers, Fibers 10 (2022), https://doi.org/10.3390/fib10060052.
[19] N. Vidakis, M. Petousis, A. Maniadi, E. Koudoumas, G. Kenanakis, C. Romanitan, O. Tutunaru, M. Suchea, J. Kechagias, The mechanical and physical properties of 3D-printed materials composed of ABS-ZnO nanocomposites and ABS-ZnO microcomposites, Micromachines 11 (2020) 1–20, https://doi.org/10.3390/mi11060615.
[20] A. Joseph Arockiam, Karthikeyan Subramanian, R.G. Padmanabhan, Rajeshkumar Selvaraj, Dilip Kumar Bagal, S. Rajesh, A review on PLA with different fillers used as a filament in 3D printing, Mater. Today Proc. 50 (2022) 2057–2064, https://doi.org/10.1016/j.matpr.2021.09.413.
[21] M.R. Khosravani, F. Berto, M.R. Ayatollahi, T. Reinicke, Characterization of 3D-printed PLA parts with different raster orientations and printing speeds, Sci. Rep. 12 (2022) 1016, https://doi.org/10.1038/s41598-022-05005-4.
[22] G. Atakok, M. Kam, H.B. Koc, Tensile, three-point bending and impact strength of 3D printed parts using PLA and recycled PLA filaments: a statistical investigation, J. Mater. Res. Technol. 18 (2022) 1542–1554, https://doi.org/10.1016/j.jmrt.2022.03.013.
[23] N. Vidakis, M. Petousis, J.D. Kechagias, A comprehensive investigation of the 3D printing parameters' effects on the mechanical response of polycarbonate in fused filament fabrication, Prog. Addit. Manuf. 7 (2022) 713–722, https://doi.org/10.1007/s40964-021-00258-3.
[24] J.D. Kechagias, N. Vidakis, M. Petousis, Parameter effects and process modeling of FFF-TPU mechanical response, Mater. Manuf. Process. 38 (2021) 341–351, https://doi.org/10.1080/10426914.2021.2001523.

[25] N. Vidakis, M. Petousis, J.D. Kechagias, Parameter effects and process modelling of Polyamide 12 3D-printed parts strength and toughness, Mater. Manuf. Process. 37 (2022) 1358–1369, https://doi.org/10.1080/10426914.2022.2030871.
[26] Y. Li, Y. Lou, Tensile and bending strength improvements in PEEK parts using fused deposition modelling 3D printing considering multi-factor coupling, Polymers 12 (2020), https://doi.org/10.3390/polym12112497 (Basel).
[27] S. Xiaoyong, C. Liangcheng, M. Honglin, G. Peng, B. Zhanwei, L. Cheng, Experimental analysis of high temperature PEEK materials on 3D printing test, 2017 9th Int. Conf. Meas. Technol. Mechatronics Autom. (2017) 13–16, https://doi.org/10.1109/ICMTMA.2017.0012.
[28] B. Hu, X. Duan, Z. Xing, Z. Xu, C. Du, H. Zhou, R. Chen, B. Shan, Improved design of fused deposition modeling equipment for 3D printing of high-performance PEEK parts, Mech. Mater. 137 (2019), 103139, https://doi.org/10.1016/j.mechmat.2019.103139.
[29] J.M. Toth, in: S.M.B.T.-P.B.H. (Second E. Kurtz (Ed.), Chapter 8 - Biocompatibility of PEEK Polymers, Plast. Des. Libr., William Andrew Publishing, 2019, pp. 107–119, https://doi.org/10.1016/B978-0-12-812524-3.00008-9.
[30] J. Zheng, H. Zhao, E. Dong, J. Kang, C. Liu, C. Sun, D. Li, L. Wang, Additively-manufactured PEEK/HA porous scaffolds with highly-controllable mechanical properties and excellent biocompatibility, Mater. Sci. Eng. C. 128 (2021), 112333, https://doi.org/10.1016/j.msec.2021.112333.
[31] B.I. Oladapo, S.A. Zahedi, S.O. Ismail, F.T. Omigbodun, 3D printing of PEEK and its composite to increase biointerfaces as a biomedical material- A review, Colloids Surf. B Biointerfaces 203 (2021), 111726, https://doi.org/10.1016/j.colsurfb.2021.111726.
[32] N. Sharma, S. Aghlmandi, F. Dalcanale, D. Seiler, H.-F. Zeilhofer, P. Honigmann, F.M. Thieringer, Quantitative assessment of point-of-care 3D-printed patient-specific polyetheretherketone (PEEK) cranial implants, Int. J. Mol. Sci. 22 (2021), https://doi.org/10.3390/ijms22168521.
[33] C. Basgul, F.M. Thieringer, S.M. Kurtz, Heat transfer-based non-isothermal healing model for the interfacial bonding strength of fused filament fabricated polyetheretherketone, Addit. Manuf. 46 (2021), 102097, https://doi.org/10.1016/j.addma.2021.102097.
[34] K. Elhattab, P. Sikder, J.M. Walker, M.C. Bottino, S.B. Bhaduri, Fabrication and evaluation of 3-D printed PEEK scaffolds containing Macropores by design, Mater. Lett. 263 (2020), 127227, https://doi.org/10.1016/j.matlet.2019.127227.
[35] Z. Liu, M. Zhang, Z. Wang, Y. Wang, W. Dong, W. Ma, S. Zhao, D. Sun, 3D-printed porous PEEK scaffold combined with CSMA/POSS bioactive surface: a strategy for enhancing osseointegration of PEEK implants, Compos. B Eng. 230 (2022), 109512, https://doi.org/10.1016/j.compositesb.2021.109512.
[36] B.I. Oladapo, S.A. Zahedi, S.O. Ismail, F.T. Omigbodun, O.K. Bowoto, M.A. Olawumi, M.A. Muhammad, 3D printing of PEEK–cHAp scaffold for medical bone implant, Bio-Design Manuf. 4 (2021) 44–59, https://doi.org/10.1007/s42242-020-00098-0.
[37] P. Feng, J. Jia, S. Peng, W. Yang, S. Bin, C. Shuai, Graphene oxide-driven interfacial coupling in laser 3D printed PEEK/PVA scaffolds for bone regeneration, Virtual Phys. Prototyp. 15 (2020) 211–226, https://doi.org/10.1080/17452759.2020.1719457.
[38] N. Sinha, N. Gupta, K.M. Reddy, Y.M. Shastry, Versatility of PEEK as a fixed partial denture framework, J. Indian Prosthodont. Soc. 17 (2017) 80–83, https://doi.org/10.4103/0972-4052.197941.
[39] A.D. Schwitalla, M. Abou-Emara, T. Spintig, J. Lackmann, W.D. Müller, Finite element analysis of the biomechanical effects of PEEK dental implants on the peri-implant bone, J. Biomech. 48 (2015) 1–7, https://doi.org/10.1016/j.jbiomech.2014.11.017.
[40] C. Lu, N. Xu, T. Zheng, X. Zhang, H. Lv, X. Lu, L. Xiao, D. Zhang, The optimization of process parameters and characterization of high-performance CF/PEEK composites prepared by flexible CF/PEEK plain weave fabrics, Polymers 11 (2019), https://doi.org/10.3390/polym11010053.
[41] I.V. Panayotov, V. Orti, F. Cuisinier, J. Yachouh, Polyetheretherketone (PEEK) for medical applications, J. Mater. Sci. Mater. Med. 27 (2016) 118, https://doi.org/10.1007/s10856-016-5731-4.
[42] C. Yang, X. Tian, D. Li, Y. Cao, F. Zhao, C. Shi, Influence of thermal processing conditions in 3D printing on the crystallinity and mechanical properties of PEEK material, J. Mater. Process. Technol. 248 (2017) 1–7, https://doi.org/10.1016/j.jmatprotec.2017.04.027.
[43] W. Wu, P. Geng, G. Li, D. Zhao, H. Zhang, J. Zhao, Influence of layer thickness and raster angle on the mechanical properties of 3D-printed PEEK and a comparative mechanical study between PEEK and ABS, Materials 8 (2015) 5834–5846, https://doi.org/10.3390/ma8095271.
[44] C.Y. Liaw, J.W. Tolbert, L.W. Chow, M. Guvendiren, Interlayer bonding strength of 3D printed PEEK specimens, Soft Matter 17 (2021) 4775–4789, https://doi.org/10.1039/d1sm00417d.
[45] M. Vaezi, S. Yang, Extrusion-based additive manufacturing of PEEK for biomedical applications, Virtual Phys. Prototyp. 10 (2015) 123–135, https://doi.org/10.1080/17452759.2015.1097053.
[46] A. El Magri, K. El Mabrouk, S. Vaudreuil, H. Chibane, M.E. Touhami, Optimization of printing parameters for improvement of mechanical and thermal performances of 3D printed poly(ether ether ketone) parts, J. Appl. Polym. Sci. 137 (2020), 49087, https://doi.org/10.1002/app.49087.
[47] M. Rinaldi, T. Ghidini, F. Cecchini, A. Brandao, F. Nanni, Additive layer manufacturing of poly (ether ether ketone) via FDM, Compos. B Eng. 145 (2018) 162–172, https://doi.org/10.1016/j.compositesb.2018.03.029.
[48] B. Hu, Z. Xing, W. Wu, X. Zhang, H. Zhou, C. Du, B. Shan, Enhancing the mechanical properties of SCF/PEEK composites in FDM via process-parameter optimization, High Perform. Polym. 33 (2021) 914–923, https://doi.org/10.1177/09540083211003654.
[49] P. Wang, B. Zou, S. Ding, C. Huang, Z. Shi, Y. Ma, P. Yao, Preparation of short CF/GF reinforced PEEK composite filaments and their comprehensive properties evaluation for FDM-3D printing, Compos. B Eng. 198 (2020), 108175, https://doi.org/10.1016/j.compositesb.2020.108175.
[50] K. Rodzeń, P.K. Sharma, A. McIlhagger, M. Mokhtari, F. Dave, D. Tormey, R. Sherlock, B.J. Meenan, A. Boyd, The direct 3D printing of functional PEEK/hydroxyapatite composites via a fused filament fabrication approach, Polymers 13 (2021), https://doi.org/10.3390/polym13040545.
[51] C.-P. Jiang, Y.-C. Cheng, H.-W. Lin, Y.-L. Chang, T. Pasang, S.-Y. Lee, Optimization of FDM 3D printing parameters for high strength PEEK using the Taguchi method and experimental validation, Rapid Prototyp. J. 28 (2022) 1260–1271, https://doi.org/10.1108/RPJ-07-2021-0166.
[52] T. Mohamed, N. Barhoumi, K. Lamnawar, A. Maazouz, A. Znaidi, Optimization of fused deposition modeling process parameters using the Taguchi method to improve the tensile properties of 3D-printed polyether ether ketone, Proc. Inst. Mech. Eng. Part L J. Mater. Des. Appl. 235 (2021) 2565–2573, https://doi.org/10.1177/14644207211017572.
[53] Y. Wang, W.-D.D. Müller, A. Rumjahn, F. Schmidt, A.D. Schwitalla, Mechanical properties of fused filament fabricated PEEK for biomedical applications depending on additive manufacturing parameters, J. Mech. Behav. Biomed. Mater. 115 (2021), 104250, https://doi.org/10.1016/j.jmbbm.2020.104250.
[54] H. Liu, X. Cheng, X.H. Yang, G.M. Zheng, Q.J. Guo, Experimental study on parameters of 3D printing process for PEEK materials, IOP Conf. Ser. Mater. Sci. Eng. 504 (2019), 12001, https://doi.org/10.1088/1757-899X/504/1/012001.
[55] K. Kim, H. Noh, K. Park, H.W. Jeon, S. Lim, Characterization of power demand and energy consumption for fused filament fabrication using CFR-PEEK, Rapid Prototyp. J. 28 (2022) 1394–1406, https://doi.org/10.1108/RPJ-07-2021-0188.
[56] M.R. Hassan, H.W. Jeon, G. Kim, K. Park, The effects of infill patterns and infill percentages on energy consumption in fused filament fabrication using CFR-PEEK, Rapid Prototyp. J. 27 (2021) 1886–1899, https://doi.org/10.1108/RPJ-11-2020-0288.
[57] J.D. Kechagias, N. Vidakis, Parametric optimization of material extrusion 3D printing process: an assessment of Box-Behnken vs. full-factorial experimental approach, Int. J. Adv. Manuf. Technol. 121 (2022) 3163–3172, https://doi.org/10.1007/s00170-022-09532-2.
[58] Y. Wang, W.-D. Müller, A. Rumjahn, A. Schwitalla, Parameters influencing the outcome of additive manufacturing of tiny medical devices based on PEEK, Materials 13 (2020), https://doi.org/10.3390/ma13020466.
[59] W.-K. Jung, H. Kim, Y.-C. Park, J.-W. Lee, S.-H. Ahn, Smart sewing work measurement system using IoT-based power monitoring device and approximation algorithm, Int. J. Prod. Res. 58 (2020) 6202–6216, https://doi.org/10.1080/00207543.2019.1671629.
[60] Z. Liu, B. Bhandari, S. Prakash, M. Zhang, Creation of internal structure of mashed potato construct by 3D printing and its textural properties, Food Res. Int. 111 (2018) 534–543, https://doi.org/10.1016/j.foodres.2018.05.075.
[61] R.F. Quero, G. da Silveira, J.A. da Silva, D.P. de Jesus, Understanding and improving FDM 3D printing to fabricate high-resolution and optically transparent microfluidic devices, Lab Chip 21 (2021) 3715–3729, https://doi.org/10.1039/D1LC00518A.
[62] Karin Kandananond, Surface roughness prediction of FFF-fabricated workpieces by artificial neural network and Box-Behnken method, Int. J. Metrol. Qual. Eng. 12 (2021) 17, https://doi.org/10.1051/ijmqe/2021014.

[63] R.M. R, V. R, R. S, Experimental analysis on density, micro-hardness, surface roughness and processing time of acrylonitrile butadiene styrene (ABS) through fused deposition modeling (FDM) using box behnken design (BBD), mater, Today Commun 27 (2021), 102353, https://doi.org/10.1016/j.mtcomm.2021.102353.
[64] J.D. Kechagias, N. Vidakis, Parametric optimization of material extrusion 3D printing process : an assessment of Box - behnken vs . full - factorial experimental approach, Int. J. Adv. Manuf. Technol. 121 (2022) 3163–3172, https://doi.org/10.1007/s00170-022-09532-2.
[65] N. Vidakis, M. Petousis, N. Mountakis, A. Moutsopoulou, E. Karapidakis, Energy consumption vs . Tensile strength of poly [ methyl methacrylate ] in material extrusion 3D printing : the impact of six control settings, Polymers 15 (2023) 845, https://doi.org/10.3390/polym15040845.
[66] M. Petousis, N. Vidakis, N. Mountakis, E. Karapidakis, A. Moutsopoulou, Functionality versus sustainability for PLA in MEX 3D printing : the impact of generic process control factors on flexural response and energy efficiency, Polymers 15 (2023) 1232, https://doi.org/10.3390/polym15051232.
[67] M. Petousis, N. Vidakis, N. Mountakis, E. Karapidakis, A. Moutsopoulou, Compressive response versus power consumption of acrylonitrile butadiene styrene in material extrusion additive manufacturing : the impact of seven critical control parameters, Int. J. Adv. Manuf. Technol. (2023), https://doi.org/10.1007/s00170-023-11202-w.
[68] M. Sadegh, A. Parast, A. Bagheri, A. Kami, M. Azadi, M.S.A. Parast, A. Bagheri, A. Kami, M. Azadi, V. Asghari, M. Sadegh, A. Parast, A. Bagheri, A. Kami, M. Azadi, Bending fatigue behavior of fused filament fabrication 3D-printed ABS and PLA joints with rotary friction welding, Prog. Addit. Manuf. 7 (2022) 1345–1361, https://doi.org/10.1007/s40964-022-00307-5.
[69] Q. Li, W. Zhao, Y. Li, W. Yang, G. Wang, Flexural properties and fracture behavior of CF/PEEK in orthogonal building orientation by FDM: microstructure and mechanism, Polymers 11 (2019) 656, https://doi.org/10.3390/polym11040656.
[70] M.R. Khosravani, T. Reinicke, Fracture behavior of intact and defected 3D-printed parts, Procedia Struct. Integr. 31 (2021) 105–110, https://doi.org/10.1016/j.prostr.2021.03.017.
[71] M.R. Khosravani, A. Zolfagharian, Fracture and load-carrying capacity of 3D-printed cracked components, Extrem. Mech. Lett. 37 (2020), 100692, https://doi.org/10.1016/j.eml.2020.100692.
[72] B. Ameri, F. Taheri-Behrooz, M.R.M. Aliha, Evaluation of the geometrical discontinuity effect on mixed-mode I/II fracture load of FDM 3D-printed parts, Theor. Appl. Fract. Mech. 113 (2021), 102953, https://doi.org/10.1016/j.tafmec.2021.102953.
[73] M.R. Khosravani, S. Rezaei, H. Ruan, T. Reinicke, Fracture behavior of anisotropic 3D-printed parts: experiments and numerical simulations, J. Mater. Res. Technol. 19 (2022) 1260–1270, https://doi.org/10.1016/j.jmrt.2022.05.068.
[74] N. Aliheidari, R. Tripuraneni, A. Ameli, S. Nadimpalli, Fracture resistance measurement of fused deposition modeling 3D printed polymers, Polym. Test. 60 (2017) 94–101, https://doi.org/10.1016/j.polymertesting.2017.03.016.
[75] J. Allum, A. Gleadall, V.V. Silberschmidt, Fracture of 3D-printed polymers: crucial role of filament-scale geometric features, Eng. Fract. Mech. 224 (2020), 106818, https://doi.org/10.1016/j.engfracmech.2019.106818.
[76] A. Zolfagharian, M.R. Khosravani, A. Kaynak, Fracture resistance analysis of 3D-printed polymers, Polymers 12 (2020), https://doi.org/10.3390/polym12020302.
[77] A.R. Torrado Perez, D.A. Roberson, R.B. Wicker, Fracture surface analysis of 3D-printed tensile specimens of novel ABS-based materials, J. Fail. Anal. Prev. 14 (2014) 343–353, https://doi.org/10.1007/s11668-014-9803-9.
[78] A. Nurizada, K. Kirane, Induced anisotropy in the fracturing behavior of 3D printed parts analyzed by the size effect method, Eng. Fract. Mech. 239 (2020), 107304, https://doi.org/10.1016/j.engfracmech.2020.107304.
[79] S.S. Singh, P. Chakraborty, R. Kitey, Deformation characteristics of glass-filled epoxy composite under compression: role of filler shape and volume fraction, Polym. Compos. 40 (2019) 4726–4741, https://doi.org/10.1002/pc.25341.
[80] J. Chen, A.J. Kinloch, S. Sprenger, A.C. Taylor, The mechanical properties and toughening mechanisms of an epoxy polymer modified with polysiloxane-based core-shell particles, Polymer (Guildf) 54 (2013) 4276–4289, https://doi.org/10.1016/j.polymer.2013.06.009.
[81] Ratnesh Raj, Rai Dixit Amit, Sarthak S. Singh, Sudeepto Paul, Print parameter optimization and mechanical deformation analysis of Alumina-nanoparticle doped photocurable nanocomposites fabricated using vat-photopolymerization based additive technology, Addit. Manuf. (2022), https://doi.org/10.1016/j.addma.2022.103201.
[82] P. Wang, B. Zou, H. Xiao, S. Ding, C. Huang, Effects of printing parameters of fused deposition modeling on mechanical properties, surface quality, and microstructure of PEEK, J. Mater. Process. Technol. 271 (2019) 62–74, https://doi.org/10.1016/j.jmatprotec.2019.03.016.
[83] P.M. (Ed. . Swamidass, MAPE (mean absolute percentage error)MEAN ABSOLUTE PERCENTAGE ERROR (MAPE) BT - Encyclopedia of Production and Manufacturing Management, in: P.M. Swamidass (Ed.), Springer US, Boston, MA, USA, 2000: p. 462. https://doi.org/10.1007/1-4020-0612-8_580.